ANL/CP--77116

DE92 041104

Dynamic Stability of Maglev Systems

by

Y. Cai, S. S. Chen, T. M. Mulcahy, and D. M. Rote
Argonne National Laboratory
9700 South Cass Avenue, Argonne, Illinois 60439

For presentation at the 63rd Shock and Vibration Symposium, October 27–29, 1992, Las Cruces, NM.

*Work performed under the sponsorship of the U.S. Army Corps of Engineers and the Federal Railroad Administration through interagency agreements with the U.S. Department of Energy.

Dynamic Stability of Maglev Systems

by

Y. Cai, S. S. Chen, T. M. Mulcahy, and D. M. Rote

Abstract

Since the occurrence of dynamic instabilities is not acceptable for any commercial maglev systems, it is important to consider the dynamic instability in the development of all maglev systems. This study is to consider the stability of maglev systems based on experimental data, scoping calculations and simple mathematical models. Divergence and flutter are obtained for coupled vibration of a three-degree-of-freedom maglev vehicle on the guideway which consists of double L-shaped aluminum segments attached to a rotating wheel. The theory and analysis developed in this study provides basic stability characteristics and identifies future research needs for maglev system.

1 Introduction

The dynamic response of maglev systems is important in several respects: safety and ride quality, guideway design, and cost of maglev systems. Ride quality is determined by the response of vehicles as well as other environmental factors, such as humidity and noise. The dynamic response of vehicles is the key element in the determination of ride quality, and vehicle stability of is one of the important elements relative to safety. In order to design a proper guideway to achieve an acceptable ride quality in the stable region, the dynamics of vehicles must be understood. Furthermore, the tradeoff between the guideway smoothness and

levitation and control systems must be considered to make maglev systems economically feasible. The link between guideway and other maglev components is the vehicle dynamics. For a commercial maglev system, the detailed vehicle dynamics must be analyzed and tested.

For safety reason, maglev systems should be stable without active controls. Magnetic forces are basically position–dependent, while some of the magnetic forces are also velocity–dependent. These motion–dependent magnetic forces can induce various types of instability. In addition, in some cases, the periodic structure of the motion–dependent magnetic forces may also induce parametric resonance and combination resonance.

Some analytical and experimental studies have been performed to understand the stability characteristics of maglev systems. Several examples are summarized briefly as follows:

Theoretical Studies

- Davis and Wilkie (1971) studied a magnetic coil moving over a conducting track and concluded that negative damping occurs for velocities greater than the characteristic velocity based on thin track theory.

- Ohno et al. (1973) studied the pulsating lift forces in a linear synchronous motor. These pulsating forces may cause parametric resonance and combination resonance in addition to the heave and pitch oscillations.

- Baiko et al. (Chu and Moon 1983) considered the interactions of the induced eddy currents with on-board superconducting magnets and found possible heave instabilities.

Experimental Studies

- An experimental vehicle floating above a large rotating wheel was found by Moon (1974) to have sway-yaw instabilities.

- Experiments performed at MIT on a test track showed the pitch-heave instability (Moon 1975).

Experimental/Analytical Studies

- A conducting guideway, consisting of L-shaped aluminum segments attached to a rotating wheel to simulate the Japanese full scale guideway at Miyazaki, was studied experimentally and analytically by Chu and Moon (1983). Divergence and flutter are obtained for coupled yaw-lateral vibration; the divergence leads to two stable equilibrium yaw positions and the flutter instability leads to a limit cycle of coupled yaw and lateral motions in the neighborhood of the drag peak.

- The variation of the magnetic lift force due to the variation of the levitated height corresponding to the sinusoidal guideway roughness was studied by Yabuno et al. (1989). Parametric resonance of the heaving and pitching motions are possible.

Based on the published analytical results and experimental data, it is obvious that different types of dynamic instabilities can occur in maglev systems. Since the occurrence of dynamic instabilities is not acceptable for any commercial maglev systems, it is important to consider the dynamic instability in the development of all maglev systems.

This study is to consider the stability of maglev systems based on experimental data, scoping calculations and simple mathematical models. The objective is to provide some basic stability characteristics and to identify future research needs.

2 Motion–Dependent Magnetic Forces

2.1 Motion–Dependent Magnetic–Force Coefficients

Magnetic forces are needed for any vehicle dynamics analysis, guideway structural design, design of fastenings, and prediction of ride quality. These force components are considered from the standpoint of vehicle stability.

As an example, consider a vehicle with six degrees of freedom, three translations, u_x, u_y, u_z and three rotation, ω_x, ω_y, ω_z, as shown in Fig. 1. Let U be the vector consisting of the six motion components; i.e.,

$$U = \begin{Bmatrix} u_1 \\ u_2 \\ u_3 \\ u_4 \\ u_5 \\ u_6 \end{Bmatrix} = \begin{Bmatrix} u_x \\ u_y \\ u_z \\ \omega_x \\ \omega_y \\ \omega_z \end{Bmatrix}. \tag{1}$$

The velocity and acceleration are given by

$$\dot{U} = \frac{\partial U}{\partial t},$$

and (2)

$$\ddot{U} = \frac{\partial^2 U}{\partial t^2}.$$

The motion–dependent magnetic forces can be written

$$f_i = \sum_{j=1}^{6} \left(m_{ij}\ddot{u}_j + c_{ij}\dot{u}_j + k_{ij}u_j \right). \tag{3}$$

where m_{ij}, c_{ij}, and k_{ij} are magnetic mass, damping, and stiffness coefficients. These coefficients can be obtained analytically, numerically, or experimentally, and are functions of the system parameters.

1. Analytical Studies: Analyses for simple cases can be performed to determine the characteristics of these coefficients. For example, an analytical method may be used to identify the coefficients which can be neglected under specific conditions.

2. Numerical Methods: For the general case with complicated geometries, analytical methods many not be appropriate and numerical methods will be more useful. Numerical methods, finite element method and boundary element method, can be used to calculate the values of all coefficients under specific conditions.

3. Experimental Techniques: Measurements of magnetic forces will give the information required to calculate magnetic–force coefficients.

2.2 Experimental Methods to Measure Motion–Dependent Magnetic–Force Coefficients

Quasi–static Motion Theory: The magnetic forces acting on an oscillating vehicle are equal, at any instant in time, to those of the same vehicle moving with a constant velocity with specific clearances equal to the actual instantaneous values. The magnetic forces depend on the deviation from a reference state of speed and clearance; i.e., the motion–dependent magnetic forces depend only on u_j, but not $\dot{u}_j$ and $\ddot{u}_j$, so that

$$f_i = \sum_{j=1}^{6} k_{ij} u_j. \tag{4}$$

In this case, the magnetic forces are determined uniquely by the vehicle position. All elements of magnetic stiffness k_{ij} can be obtained. To determine k_{ij}, the magnetic force component f_i is measured as a function of u_j. The stiffness, k_{ij}, is given by

$$k_{ij} = \frac{\partial f_i}{\partial u_j}. \tag{5}$$

In general k_{ij} is a function of U.

Unsteady Motion Theory: The magnetic forces acting on an oscillating vehicle will depend on U, $\dot{U}$, and $\ddot{U}$. The magnetic force based on the unsteady motion theory can be obtained by measuring the magnetic force acting on the vehicle oscillating in the magnetic field. For example, if the displacement component u_j is excited, its displacement is given by

$$u_j = \bar{u}_j \exp\left(\sqrt{-1}\,\omega t\right). \tag{6}$$

The motion–dependent magnetic force of the component f_i acting on the vehicle is given by

$$f_i = \left[a_{ij}\cos\left(\psi_{ij}\right) + \sqrt{-1}\,a_{ij}\sin\left(\psi_{ij}\right)\right]\bar{u}_j \exp\left(\sqrt{-1}\,\omega t\right), \tag{7}$$

where a_{ij} is the magnetic force amplitude and ψ_{ij} is the phase angle between the magnetic force and the vehicle displacement u_j. These values are measured experimentally.

Using Eqs. 3 and 6, we can also write the motion–dependent magnetic force component as

$$f_i = \left(-m_{ij}\omega^2 + \sqrt{-1}\,\omega\, c_{ij} + k_{ij}\right)\bar{u}_j \exp\left(\sqrt{-1}\,\omega t\right). \tag{8}$$

Comparing Eqs. 7 and 8 yields

$$\begin{aligned} c_{ij} &= a_{ij}\sin\left(\psi_{ij}\right)/\omega, \\ m_{ij} &= \left[k_{ij} - a_{ij}\cos\left(\psi_{ij}\right)\right]/\omega^2. \end{aligned} \tag{9}$$

Based on Eqs. 5 and 9, all motion–dependent magnetic–force matrices can be determined from two experiments: quasi–static motion and unsteady motion.

If m_{ij} and c_{ij} are of no concern, the experiment using quasi–steady motion is sufficient to determine k_{ij}.

2.3 Quasi-Static Motion–Dependent Magnetic–Force Coefficients of Maglev System with L-Shaped Guideway

An experiment, to investigate the lift, drag and guidance magnetic forces on an NdFeB permanent magnet moving over an aluminum (6061-T6) L-shaped ring which is mounted on the top surface of a 1.2-m diameter rotating wheel (shown in Fig. 2), was conducted at Argonne National Laboratory recently. For a given rotating speed of the wheel, the lift and guidance magnetic forces were measured as the guidance gap Y* and lift height h were varied. Figures 3a-3h show those measured forces as a function of h, with Y* fixed (Y* = 5 mm and 12.7 mm), or as a function of Y* with h fixed (h = 7 mm and 12.7 mm) when the surface velocity of the lateral leg of the guideway is 36.1 m/s, the highest velocity tested.

During testing, the long side of the 25.4 x 50.4 x 6.35-mm rectangular magnet was oriented parallel to the direction of motion of the L-shaped guideway and was held stationary by a two-component force transducer, comprised of two BLH C2G1 load cells connected in series to measure the lift and guidance forces simultaneously. Laboratory weights were used to calibrate the transducer and assess crosstalk, which was found to be less than 2%. The base of the load cell assembly was mounted on motorized stages, which provided accurate positioning (±0.05 mm). The out of roundness of the L-shaped guideway ring varied, but was always less than ±0.15 mm for the lateral leg and ±0.35 mm for the vertical leg. Ability to exactly position the magnet with respect to the guideway dominated our experimental error, estimated at ±5%. Previously, force measurements were made by Mulcahy et al. (1993) with the same magnet centered over a flat aluminum strip that showed [1] it to be equivalent to a single 25.4 x 50.8-mm rectangular coil of wire with a current of 6000 A, located at the center height of the magnet.

The qualitative trends in the lift and guidance force data taken at lower velocities for the L-shaped are the same as shown in Figs. 3a-3h for the highest velocity tested, which have two interesting features. First, a maximum occurs in the variation of the guidance force with respect to variations in height at a fixed gap, as shown in Figs. 3e and 3f, that is caused by the corner region of the guideway. Second, a minimum occurs in the variation of the guidance force with respect to variations in the gap at a fixed height, as shown in Figs. 3g and 3h, that is caused by the edge of the lateral leg of the guideway. As will be shown in 4.4, the first feature is associated with a flutter and the second with a divergence instability.

Based on the magnetic force data shown in Fig. 3 we can calculate the quasi-static motion-dependent magnetic-force coefficients with Eq. 5. All elements of magnetic stiffness $k_{\ell\ell}$, $k_{\ell g}$, $k_{g\ell}$ and k_{gg}, were calculated and are shown in Fig. 4 with various Y* and h.

The curve fit to both magnetic forces and stiffnesses were derived using polynomial expressions (results are given in Figs. 3 and 4) and input into a computer code to simulate coupled vibrations of maglev vehicle.

3 Stability of Maglev Systems

Without motion–dependent magnetic forces, the equation of motion for the vehicle can be written,

$$[M_v]\{\ddot{U}\}+[C_v]\{\dot{U}\}+[K_v]\{U\}=\{Q\}, \tag{10}$$

where M_V is the vehicle mass matrix, C_V is vehicle damping matrix, K_V is vehicle stiffness matrix, and Q is generalized excitation force.

The motion–dependent magnetic forces are given in Eq. 3. With motion–dependent magnetic forces, Eq. 10 becomes

$$[M_v + M_m]\{\ddot{U}\} + [C_v + C_m]\{\dot{U}\} + [K_v + K_m]\{U\} = \{Q\}, \tag{11}$$

where M_m is the magnetic mass matrix, C_m is magnetic damping matrix, and K_m is magnetic stiffness; their elements are m_{ij}, c_{ij}, and k_{ij}.

Once the magnetic–force coefficients are known, it is straightforward to analyze the stability of a vehicle. Equation 11 may be written as

$$[M]\{\ddot{U}\} + [C]\{\dot{U}\} + [K]\{U\} = \{Q\}. \tag{12}$$

In general, M, C, and K are functions of U, $\dot{U}$, and $\ddot{U}$; therefore, a complete solution is rather difficult to obtain. In many practical situations, one can ignore all nonlinear terms, such that M, C, and K are independent of vehicle motion.

By premultiplying by $\{\dot{U}\}^T$ and forming the symmetric and antisymmetric components of the matrices

$$\begin{aligned}
[M_1] &= \frac{1}{2}\left([M] + [M]^T\right), \qquad [M_2] = \frac{1}{2}\left([M] - [M]^T\right), \\
[C_1] &= \frac{1}{2}\left([C] + [C]^T\right), \qquad [C_2] = \frac{1}{2}\left([C] - [C]^T\right), \\
[K_1] &= \frac{1}{2}\left([K] + [K]^T\right), \qquad [K_2] = \frac{1}{2}\left([K] - [K]^T\right),
\end{aligned} \tag{13}$$

the terms may be separated, giving

$$\begin{aligned}
&\{\dot{U}\}^T[M_1]\{\ddot{U}\} + \{\dot{U}\}^T[C_2]\{\dot{U}\} + \{\dot{U}\}^T[K_1]\{U\} \\
&\quad = -\left(\{\dot{U}\}^T[M_2]\{\ddot{U}\} + \{\dot{U}\}^T[C_1]\{\dot{U}\} + \{\dot{U}\}^T[K_2]\{U\}\right).
\end{aligned} \tag{14}$$

Equation 14 equates rates of work. Those terms on the right–hand side of the equation produce a net work resultant when integrated over a closed path through the space {U}, the magnitude depending on the path taken. The forces corresponding to the matrices M_2, C_1, and K_2, appearing on the right–hand side, are thus by definition the nonconservative parts of the forces represented by M, C, and K. The terms on the left–hand side similarly can be shown to give rise to a zero work–resultant over any closed path, and therefore together are the sum of the rates of work from the potential forces and the rate of change of kinetic energy. Different types of instability can be classified according to the dominant terms in Eq. 14.

- Magnetic Damping Controlled Instability (single mode flutter): The dominant terms are associated with the symmetric damping matrix $[C_1]$. Flutter arises because the magnetic damping forces create "negatic damping," that is, a magnetic force that acts in phase with the vehicle velocity.

- Magnetic Stiffness Controlled Instability (coupled mode flutter): The dominant terms are associated with the antisymmetric stiffness matrix $[K_2]$. It is called coupled mode flutter because a minimum of two modes are required to produce it.

Corresponding to the single–mode flutter and coupled–mode flutter, there may exist parametric resonance and combination resonance if the motion–dependent magnetic forces are a periodic function of time.

- Parametric Resonance: When the period of a motion–dependent magnetic force is a multiple of one of the natural frequencies of the vehicle, the vehicle may be dynamically unstable.

- Combination Resonance: When the period of the motion–dependent magnetic forces is equal to the sum or difference divided by an integer of the natural frequencies of the vehicle, the vehicle may also be subjected to dynamic instability.

In practical cases, two or more mechanisms may interact with one another and Eq. 12 is applicable for general cases.

4 Simplified Vehicle Models for Dynamic Instability

Different vehicles are considered to understand the stability characteristics.

4.1 A Two–Degree–of–Freedom Vehicle

A maglev vehicle is supported by magnetic forces; the resultant lift and drag forces of the coil above the continuous sheet track can be represented approximately by (Sinha 1987)

$$
\begin{aligned}
&F_L(v,z,t) = \varepsilon_L F(t),\\
&F_D(v,z,t) = \varepsilon_D F(t),\\
&F(t) = \mu_o I^2/4\pi z,\\
&\varepsilon_L = 1 - 1/(1 + v^2/w^2)^n,\\
&\varepsilon_D = (w/v)[1 - 1/(1 + v^2/w^2)^n],\\
&w = 2/\mu_o \sigma h.
\end{aligned}
\tag{15}
$$

where v is the forward velocity, z is the steady–state height of the coil above the track, t is the time, I is the constant coil current, and w is the characteristic speed and is related to the track thickness h, conductivity σ, and permeability μ_0. The value of n is 1 for a single conductor and varies from about 1/5 to 1/3 for coils (Rhodes and Mulhall 1981). Note that F(t) represents the repulsive force between the coil and its image coil. The force ratios, ε_L and ε_D, are given in Fig. 5 for n = 1, 1/3, and 1/5.

Assume that the vehicle is traveling at a velocity v_0 at an equilibrium height z_0. The instantaneous position and height of the vehicle are x and z respectively; therefore,

$$x(t) = v_0 t + X(t),$$
$$z(t) = z_0 + Z(t). \tag{16}$$

The equations of motion for the vehicle moving at a velocity v(t) with a levitation height z(t) can be written as

$$m\ddot{z}(t) = -mg + F_L(v,z,t),$$
$$m\ddot{x}(t) = F_p - F_D(v,z,t) - F_a, \tag{17}$$

where m is the mass of the vehicle, F_p is the propulsion force, and F_a is the aerodynamic force. The aerodynamic force is given by

$$F_a = K_a v^2,$$
$$K_a = 0.5\, C_D L A \rho, \tag{18}$$

$$C_{zx} = (mg/\varepsilon_L)2nv_0/[w^2(1 + v_0^2/w^2)^{n+1}],$$

$$C_{xx} = wmg/v_0^2\,[w^2 - (2n - 1)v_0^2/(w^2 + v_0^2)] + 2K_a v_0, \tag{22}$$

$$K_{zz} = mg/z_0,$$

$$K_{xz} = wmg/v_0 z_0.$$

For high speed vehicles, the values of C_{zx} and K_{xz} are approximately zero. Therefore, the motions in the vertical direction and forward direction are uncoupled at high speeds.

Equations 20 can be analyzed. Let

$$Z(t) = a\,\exp(i\omega t), \tag{23}$$

$$X(t) = b\,\exp(i\omega t).$$

Substituting Eqs. 23 into Eqs. 20 gives the following frequency equation:

$$\begin{bmatrix} -m\omega^2 + K_{zz} & -i\omega C_{zx} \\ -K_{xz} & -m\omega^2 + i\omega C_{xx} \end{bmatrix} \begin{Bmatrix} a \\ b \end{Bmatrix} = \begin{Bmatrix} 0 \\ 0 \end{Bmatrix}. \tag{24}$$

The natural frequencies can be determined from the determinant of the coefficient matrix given in Eq. 24. At high speeds, the off–diagonal terms may be neglected. The natural frequency of the vertical motion f_v is

$$f_v = (g/z_0)^{0.5}/2\pi. \tag{25}$$

The natural frequency in the vertical direction depends on the levitation height only. Figure 6 shows the natural frequency as a function of the gap. At high speeds, oscillations in the vertical direction are stable.

In the forward direction, the motion is given by

$$X(t) = C_1 + C_2\exp(st). \tag{26}$$

For high speed vehicles, the exponent s is approximately given by

$$s = (2n - 1)wg/v_o^2 - 2K_a v_o. \tag{27}$$

Note that the vehicle may be unstable if n = 1, and K_a is zero. At high speeds, the second term given in Eq. 27 is larger than the first term regardless of the values of n; therefore, s is negative and the system is stable.

4.2 A Three–Degree–of–Freedom Vehicle

Figure 7 shows a three–degree–of–freedom vehicle traveling at a velocity v_o at an equilibrium height z_o. For a symmetric vehicle the instantaneous position and height of the vehicle are x(t), $z_1(t)$, and $z_2(t)$; therefore,

$$\begin{aligned} x(t) &= v_o(t) + X(t)\,, \\ z_1(t) &= z_o + Z_1(t)\,, \\ z_2(t) &= z_o + Z_2(t)\,. \end{aligned} \tag{28}$$

The equations of motion for the vehicle moving at a velocity v(t) with levitation height $z_1(t)$ and $z_2(t)$ can be written as

$$m\ddot{x}(t) = F_p - F_{D1}(z_1, v, t) - F_{D2}(z_2, v, t) - F_a,$$

$$\frac{m}{2}[\ddot{z}_1(t)+\ddot{z}_2(t)] = -mg + F_{L1}(z_1,v,t) + F_{L2}(z_2,v,t), \tag{29}$$

$$\frac{I_\theta}{L}[\ddot{z}_1(t)-\ddot{z}_2(t)] = \frac{L}{2}[F_{L1}(z_1,v,t) - F_{L2}(z_2,v,t)].$$

where m is the vehicle mass, I_θ is the rotational moment of inertia about the vehicle's center of mass, F_p is the propulsion force, and F_a is the aerodynamic force which is assumed to act at the center of mass of the vehicle and is given by Eq. 18.

For a symmetric vehicle with two identical levitation systems at the two ends, the equilibrium point of the vehicle v_0, z_{10}, and z_{20} as well as the magnetic forces is defined as

$$\begin{aligned}
&F_{L1}(v_0,z_{10}) + F_{L2}(v_0,z_{20}) = mg\,,\\
&F_{D1}(v_0,z_{10}) + F_{D2}(v_0,z_{20}) = F_p - F_a\,,\\
&z_{10} = z_{20} = z_0\,,\\
&F_{L1}(v_0,z_{10}) = F_{L2}(v_0,z_{20})\,,\\
&F_{D1}(v_0,z_{20}) = F_{D2}(v_0,z_{20})\,.
\end{aligned} \tag{30}$$

Using Eqs. 28, 29, 30, and 18 and neglecting the nonlinear terms yields the following equations of motion of the vehicle, X(t), $Z_1(t)$, and $Z_2(t)$:

$$\begin{aligned}
&\frac{m}{2}(\ddot{Z}_1+\ddot{Z}_2) + (C_{zx1}+C_{zx2})\dot{X} + K_{zz1}Z_1 + K_{zz2}Z_2 = 0\\
&\frac{2I_\theta}{L^2}(\ddot{z}_1-\ddot{z}_2) + (C_{zx1}-C_{zx2})\dot{X} + (K_{zz1}Z_1 - K_{zz2}Z_2 = 0\\
&m\ddot{X} + (C_{xx1}+C_{xx2}+2k_a v_0)\dot{X} + K_{xz1}Z_1 + K_{xz2}Z_2 = 0
\end{aligned} \tag{31}$$

where

$$C_{zxi} = -\left.\frac{\partial F_{Li}}{\partial v}\right|_{(v_o,z_o)}$$

$$C_{xxi} = \left.\frac{\partial F_{Di}}{\partial v}\right|_{(v_o,z_o)}$$

$$K_{zzi} = -\left.\frac{\partial F_{Li}}{\partial z_i}\right|_{(v_o,z_o)} \qquad (32)$$

$$K_{xzi} = \left.\frac{\partial F_{Di}}{\partial z_i}\right|_{(v_o,z_o)}$$

$i = 1, 2.$

The magnetic damping coefficients C_{zxi} and C_{xxi}, and magnetic stiffness coefficients K_{zzi} and K_{xzi} can be calculated from the magnetic lift and drag forces given in Eq. 15.

At high speeds, K_{zxi} and C_{xzi} are approximately zero. The equations of motion become

$$\frac{m}{2}(\ddot{Z}_1 + \ddot{Z}_2) + K_{zz1}Z_1 + K_{zz2}Z_2 = 0,$$

$$\frac{2I_\theta}{L^2}(\ddot{Z}_1 - \ddot{Z}_2) + K_{zz1}Z_1 - K_{zz2}Z_2 = 0, \qquad (33)$$

$$m\ddot{X} + (C_{xx1} + C_{xx2} + 2K_a v_o)\dot{X} = 0.$$

In this case, the vehicle is stable at high speeds; this is similar to a two–degree–of–freedom vehicle. The natural frequency of vertical oscillations is the same as the two–degree–of–freedom system given in Eq. 25. The natural frequency of pitching oscillations is

$$f_p = \frac{1}{2\pi}\left(\frac{L^2 mg}{4I_\theta z_o}\right)^{0.5} . \tag{34}$$

For a square vehicle with length L and height h, the natural frequency of pitching oscillations is

$$f_p = \frac{1}{2\pi}\left(\frac{g}{z_o}\right)^{0.5}\left(\frac{3}{1+\frac{h_2}{L^2}}\right)^{0.5} . \tag{35}$$

The natural frequency of pitching oscillations is larger than vertical oscillations. For a long vehicle ($h << L$) f_p is equal to about 1.7 f_v. For a square vehicle, f_p = 1.4 f_v. At high speeds, heaving and pitching oscillations are stable for the magnetic levitation described by Eq. 15. In the forward direction, the result is the same as that for a two–degree–of–freedom vehicle.

4.3 A Six–Degree–of–Freedom Vehicle

For a six–degree–of–freedom vehicle shown in Fig. 1, the stability can be studied from Eqs. 11 or 12. Once the coefficients of magnetic forces m_{ij}, c_{ij}, and k_{ij} are known, Eqs. 11 or 12 can be evaluated for Q = 0. Let the displacement of a particular component be

$$u_j(t) = a_j \exp(\lambda + i\omega)t . \tag{36}$$

Substituting Eq. 36 into Eq. 12 with Q = 0 yield

$$\left\{(\lambda + i\omega)^2[M] + (\lambda + i\omega)[C] + [K]\right\}\{A\} = \{0\} . \tag{37}$$

The values of λ and ω can be calculated based on Eq. 37 by setting the determinant of the coefficient matrix equal to zero.

The stability of the vehicle is determined by λ, which is a function of v. If $\lambda < 0$, the vehicle motion is damped; if $\lambda > 0$, the vehicle displacement increases with time until nonlinear effects become important.

In order to solve this problem, all motion–dependent magnetic–force coefficients must be known. At this time, it appears that very little analytical, numerical, or experimental data are available. In any future maglev systems, it is necessary to investigate the characteristics of motion–dependent magnetic forces to avoid dynamic instabilities.

4.4 A Vehicle on a Double L-Shape Aluminum Sheet Guideway

Figure 8 shows the cross section of a vehicle with double L–shape aluminum sheet guideway. Assume the vehicle traveling at a constant velocity along x direction. Two permanent magnets are attached to the bottom of vehicle and provide lift and guidance force F_{L_1}, F_{L_2}, F_{G_1} and F_{G_2} (see Fig. 8). Assume at initial state, $h_1 = h_2 = h_0$ and $g_1 = g_2 = g_0$, the geometries of vehicle and guideway can be expressed as following

$$L_1 = L_2 = S = 76.2 \text{ (mm)}$$

$$W = 152.4 + S - 2g_0 \text{ (mm)}$$

$$H = 0.9\,W \text{ (mm)}$$

$$a = 0.5\ H \quad (mm)$$

$$b = 0.5(W-25.4) \quad (mm)$$

Equations of motion for this three–degree–of–freedom maglev system can be written as

$$m\ddot{z} + C\dot{z} = F_{L_1} + F_{L_2} - mg$$

$$I\ddot{\theta} + E\dot{\theta} = \left(F_{G_1} + F_{G_2}\right)a + \left(F_{G_1} + F_{G_2}\right)b \tag{38}$$

$$m\ddot{y} + D\dot{y} = F_{G_1} + F_{G_2}$$

where m is the mass of the vehicle, C and D are damping ratios; I is the moment of inertia about the center of mass inertia moment of the vehicle ($I = (m/12)(H^2+W^2)$). F_{L_1}, F_{L_2}, F_{G_1} and F_{G_2} are lift and guidance forces and are functions of y and z. At equilibrium position, they are $F_{L_{10}}(y_o,z_o)$, $F_{L_{20}}(y_o,z_o)$, $F_{G_{10}}(y_o,z_o)$ and $F_{G_{20}}(y_o,z_o)$. Apply them to Eqs. 38. These are

$$F_{L_{10}} = F_{L_{20}}$$

$$F_{L_{10}} + F_{L_{20}} = mg \tag{39}$$

$$F_{G_{10}} = -F_{G_{20}}$$

Therefore

$$m = \frac{F_{L_{10}} + F_{L_{20}}}{g} = \frac{2F_L(h_o)}{g}. \tag{40}$$

Let

$$\left.\begin{aligned} z &= \frac{1}{2}(u_1 + u_2) \\ y &= u_3 \\ \theta &= (u_1 - u_2)/2b \end{aligned}\right\}, \tag{41}$$

where u_1, u_2 and u_3 are shown in Fig. 9. Equations 38 can be rewritten as

$$\begin{aligned} m(\ddot{u}_1 + \ddot{u}_2) + c(\dot{u}_1 - \dot{u}_2) &= 2\left(F_{L_1} + F_{L_2} - mg\right) \\ \frac{I}{b}(\ddot{u}_1 - \ddot{u}_2) + \frac{E}{b}(\dot{u}_1 - \dot{u}_2) &= 2a\left(F_{G_1} + F_{G_2}\right) + 2b\left(F_{G_1} - F_{G_2}\right) \\ m\ddot{u}_3 + D\dot{u}_3 &= F_{G_1} + F_{G_2}. \end{aligned} \tag{42}$$

Note the reduced dependence of the forces on the new displacements of Eq. 41

$$\begin{aligned} F_{L_1} &= F_{L_1}(u_1, u_3) \\ F_{L_2} &= F_{L_2}(u_2, u_3) \\ F_{G_1} &= F_{G_1}(u_1, u_3) \\ F_{G_2} &= F_{G_2}(u_2, u_3). \end{aligned} \tag{43}$$

Let

$$u_i = u_{io} + v_i \qquad i = 1, 2 \tag{44}$$

The linear approximation of lift and guidance forces can be expressed as

$$
\begin{aligned}
F_{L_1} &= F_{L_{10}} + \frac{\partial F_{L_1}}{\partial v_1} v_1 + \frac{\partial F_{L1}}{\partial v_3} v_3 \\
F_{L_2} &= F_{L_{20}} + \frac{\partial F_{L_2}}{\partial v_2} v_2 + \frac{\partial F_{L2}}{\partial v_3} v_3 \\
F_{G_1} &= F_{G_{10}} + \frac{\partial F_{G_1}}{\partial v_1} v_1 + \frac{\partial F_{G1}}{\partial v_3} v_3 \\
F_{G_2} &= F_{G_{20}} + \frac{\partial F_{G_2}}{\partial v_2} v_2 + \frac{\partial F_{G2}}{\partial v_3} v_3
\end{aligned}
\tag{45}
$$

Using Eqs. 39 and 45, Eq. 42 can be rewritten as

$$
\begin{aligned}
&\ddot{v}_1 + \ddot{v}_2 + \frac{C}{m}\dot{v}_1 + \frac{C}{m}\dot{v}_2 - \frac{2}{m}\frac{\partial F_{L_1}}{\partial v_1} v_1 - \frac{2}{m}\frac{\partial F_{L_2}}{\partial v_2} v_2 - \frac{1}{m}\left(\frac{\partial F_{G_1}}{\partial v_3} + \frac{\partial F_{G_2}}{\partial v_3}\right) v_3 = 0 \\
&-\ddot{v}_1 + \ddot{v}_2 - \frac{E}{I}\dot{v}_1 + \frac{E}{I}\dot{v}_2 + \left(\frac{2cb}{I}\frac{\partial F_{L_1}}{\partial v_1} + \frac{2b^2}{I}\frac{\partial F_{G_1}}{\partial v_1}\right) v_1 \\
&\qquad + \left(\frac{2ab}{I}\frac{\partial F_{L_2}}{\partial v_2} + \frac{2b^2}{I}\frac{\partial F_{G_2}}{\partial v_2}\right) v_2 \\
&\qquad + \left[\frac{2ab}{I}\left(\frac{\partial F_{L_1}}{\partial v_3} + \frac{\partial F_{L_2}}{\partial v_3}\right) + \frac{2b^2}{I}\left(\frac{\partial F_{G_1}}{\partial v_3} + \frac{\partial F_{G_2}}{\partial v_3}\right)\right] v_3 = 0 \\
&\ddot{v}_3 + \frac{D}{m}\dot{v}_3 - \frac{1}{m}\frac{\partial F_{L_1}}{\partial v_1} v_1 - \frac{1}{m}\frac{\partial F_{L_2}}{\partial v_2} v_2 - \frac{1}{m}\left(\frac{\partial F_{L_1}}{\partial v_3} + \frac{\partial F_{L_2}}{\partial v_3}\right) v_3 = 0
\end{aligned}
\tag{46}
$$

or

$$[M]\{\ddot{v}\}+[C]\{\dot{v}\}+[K]\{v\}=0 \tag{47}$$

where

$$M=\begin{bmatrix}1 & 1 & 0\\ -1 & 1 & 0\\ 0 & 0 & 1\end{bmatrix},\qquad C=\begin{bmatrix}c_{11} & c_{22} & 0\\ c_{21} & c_{22} & 0\\ 0 & 0 & c_{23}\end{bmatrix},\qquad K=\begin{bmatrix}k_{11} & k_{12} & k_{13}\\ k_{21} & k_{22} & k_{23}\\ k_{31} & k_{32} & k_{33}\end{bmatrix}, \tag{48}$$

and

$$c_{11}=c_{12}=\frac{C}{m}$$

$$c_{21}=-c_{22}=-\frac{E}{I}$$

$$c_{33}=\frac{D}{m}$$

$$k_{11}=-\frac{2}{m}\frac{\partial F_{L_1}}{\partial v_1}$$

$$k_{12}=-\frac{2}{m}\frac{\partial F_{L_2}}{\partial v_2}$$

$$k_{13}=-\frac{1}{m}\left(\frac{\partial F_{L_1}}{\partial v_3}+\frac{\partial F_{L_2}}{\partial v_3}\right)$$

$$k_{21}=\frac{2ab}{I}\frac{\partial F_{G_1}}{\partial v_1}+\frac{2b^2}{I}\frac{\partial F_{L_1}}{\partial v_1} \tag{49}$$

$$k_{22}=\frac{2ab}{I}\frac{\partial F_{G_2}}{\partial v_2}-\frac{2b^2}{I}\frac{\partial F_{L_2}}{\partial v_2}$$

$$k_{23} = \frac{2ab}{I}\left(\frac{\partial F_{G_1}}{\partial v_3} + \frac{\partial F_{G_2}}{\partial v_3}\right) + \frac{2b^2}{I}\left(\frac{\partial F_{L_1}}{\partial v_3} + \frac{\partial F_{L_2}}{\partial v_3}\right)$$

$$k_{31} = -\frac{1}{m}\frac{\partial F_{G_1}}{\partial v_1}$$

$$k_{32} = -\frac{1}{m}\frac{\partial F_{G_2}}{\partial v_2}$$

$$k_{33} = -\frac{1}{m}\left(\frac{\partial F_{G_1}}{\partial v_3} + \frac{\partial F_{G_2}}{\partial v_3}\right)$$

where

$$\frac{\partial F_{L_1}}{\partial v_1} = k_{\ell\ell}(h), \qquad \frac{\partial F_{G_1}}{\partial v_1} = -k_{g\ell}(h),$$

$$\frac{\partial F_{L_2}}{\partial v_2} = k_{\ell\ell}(h), \qquad \frac{\partial F_{G_2}}{\partial v_2} = k_{g\ell}(h),$$

$$\frac{\partial F_{L_1}}{\partial v_3} = k_{\ell g}(g), \qquad \frac{\partial F_{G_1}}{\partial v_3} = k_{gg}(g), \tag{50}$$

$$\frac{\partial F_{L_2}}{\partial v_3} = k_{\ell g}(g), \qquad \frac{\partial F_{G_2}}{\partial v_3} = k_{gg}(g).$$

$k_{\ell\ell}(h)$, $k_{\ell g}(g)$, $k_{g\ell}(h)$ and $k_{gg}(g)$ are motion-dependent magnetic-force coefficients (see Fig. 4).

Assume the damping effects can be neglected, the eigenvalues of Eq. 47 can be obtained from

$$[K]\{v\} = \lambda [M]\{v\} \tag{51}$$

where $\lambda = \omega_R + i\,\omega_I$.

With magnetic forces and stiffnesses measured by the experiments (see Figs. 3 and 4), the eigenvalues and eigenvectors of maglev vehicle with double L-shape guideway were calculated with the theoretical model developed in this section. Some very interesting results were obtained from those calculations.

Figure 10 shows eigenvalues of vehicle motion versus levitation height varies when guidance gaps are fixed ($g_1 = g_2 = Y^* = 12.7$ mm). The first mode ω_1 shows an uncoupled heave motion, its imaginary part of eigenvalue is zero. While, the second and third modes are coupled roll-sway motions. Within range of height h = 19.0 mm to 35 mm, the imaginary parts of eigenvalues appear not to be zero. This result indicates within this range the flutter does exist for these coupled roll-yaw vibration. Table 1 and Fig. 11 give eigenvectors and modal shapes of these three modes of vehicle motion, respectively. When fixing the guidance gaps to be $g_1 = g_2 = Y^* = 5$ mm, the same results are obtained as shown in Fig. 12, there is a flutter for coupled roll-yaw modes.

Figures 13 and 14 show eigenvalues of vehicle motion versus lateral location of vehicle when $g_1 = g_2 = g_0 = 25$ mm, levitation heights h = 12.7 mm and h = 7 mm, respectively. We notice that for the third mode which presents the transversal motion of vehicle, the real part is zero and imaginary part is not zero with a certain region. It indicates that the divergence is subjected to the lateral motion of vehicle with those vehicle and guideway parameters. Figure 15 shows the real part of third mode versus lateral location of vehicle when parameter-equilibrium guidance gap varies as $g_1 = g_2 = g_0 = 10$ mm, 15 mm, 20 mm and 25 mm. We found that the divergence only appears with the case of $g_0 = 25$ mm.

We have to note that the measured and calculated data for motion-dependent magnetic-forces and force coefficients are very limited and the damping effects were not considered in above analysis. Even though the divergence and flutter appear in results of eigenvalue, we still have difficulty to completely predict dynamic instability of this three-degree-of-freedom maglev vehicle model. The further research steps are needed in modeling and understanding dynamic instability of maglev system.

5 Closing Remarks

- Motion–dependent magnetic forces are the key elements in modeling and understanding dynamic instabilities of maglev systems. At this time, it appears that very limited data are available for motion–dependent magnetic forces. Efforts will be made to compile analytical results and experimental data for motion–dependent magnetic forces. When this work is completed, recommendations will be presented on research needs on magnetic forces. In addition, specific methods to obtain motion–dependent magnetic forces will be described in detail.

- Various options can be used to stabilize a maglev system: passive electrodynamic primary suspension damping, active electrodynamic primary suspension damping, passive mechanical secondary suspension, and active mechanical secondary suspension. With a better understanding of vehicle stability characteristics, a better control law can be adopted to assure a high level of ride comfort and safety.

- Computer programs are needed in screening new system concepts, evaluation of various designs, and prediction of vehicle response. It

appears that the stability characteristics of maglev vehicles under different conditions have not been studied in detail in existing computer codes. When the information on motion–dependent magnetic forces becomes available, the existing computer codes can be significantly improved.

- Instabilities of maglev system models have been observed at Argonne and other organizations. An integrated experimental/analytical study of stability characteristics is an important part of research activities of maglev systems.

Acknowledgments

This work was performed under the sponsorship of the U. S. Army Corps of Engineers and the Federal Railroad Administration through interagency agreements with the U. S. Department of Energy.

Additional thanks to S. Winkelman for performing tests on magnetic forces.

References

Chu, D. and Moon, F. C. 1983. "Dynamic Instabilities in Magnetically Levitated Models." J. Appl. Phys. 54(3), pp. 1619-1625.

Davis, L. C., and Wilkie, D. F. 1971. "Analysis of Motion of Magnetic Levitation Systems: Implications." J. Appl. Phys. 42(12), pp. 4779-4793.

Moon, F. C. 1974. "Laboratory Studies of Magnetic Levitation in the Thin Track Limit." IEEE Trans. on Magnetics, MAG-10, No. 3, pp. 439-442 (September 1974).

Moon, F. C. 1975. "Vibration Problems in Magnetic Levitation and Propulsion." *Transport Without Wheels*, ed. by E. R. Laithwaite, Elek Science, London, pp. 122-161.

Mulcahy, T. M., Hull, J. R., Almer, J. D., and Rossing, T. D. 1993. "Edge Effects on Forces and Magnetic Fields Produced by a Conductor Moving Past a Magnet." IEEE Trans. on Magnetics (to appear).

Ohno, E., Iwamoto, M., and Yamada, T. 1973. "Characteristic of Superconductive Magnetic Suspension and Propulsion for High-Speed Trains." Proc. IEEE 61(5), pp. 579-586.

Rhodes, R. G., and Mulhall, B. E. 1981. *Magnetic Levitation for Rail Transport.* Clarendon Press Oxford, New York.

Sinha, P. K. 1987. *Electromagnetic Suspension, Dynamics and Control.* Peter Peregrinus Ltd, London, United Kingdom.

Yabuno, H., Takabayashi, Y., Yoshizawa, M., and Tsujioka, Y. 1989. "Bounding and Pitching Oscillations of a Magnetically Levitated Vehicle Caused by Guideway Roughness." Int. Conference Maglev 89, pp. 405-410.

Table 1. Eigenvectors of vehicle motion ($Y^* = 12.7$ mm)

	h = 15.0 mm			h = 25 mm			h = 37 mm		
	v_1	v_2	v_3	v_1	v_2	v_3	v_1	v_2	v_3
Uncoupled heave mode ω_1	1	1	0	1	1	0	1	1	0
Coupled roll–yaw mode ω_2	1	−1	−0.009	0.586	−0.586	−0.332	−1	1	−0.205
Coupled roll–yaw mode ω_3	−0.545	0.545	1	−0.810	0.810	0.060	1	−1	0.448

Figure Captions

1 Displacement components of a maglev system

2a Experimental apparatus for magnetic force measurement

2b Schematic for magnetic force measurement on L–shape aluminum

3 Measured lift and guidance magnetic forces

4 Measured lift and guidance magnetic stiffness

5 Magnetic forces divided by image force

6 Natural frequency as a function of levitation height

7 A three–degree–of–freedom vehicle

8 Maglev system with a vehicle over double L–shape aluminum sheet guideway

9 Displacement components of three–degree–of–freedom vehicle

10 Eigenvalues of maglev system vs. vehicle levitation height with Y* = 12.7 mm

11 Modal shapes of three–degree–of–freedom maglev system with Y* = 12.7 mm

12 Eigenvalues of maglev system vs. vehicle levitation height with Y* = 5 mm

13 Eigenvalues of maglev system vs. lateral location of vehicle with h = 12.7 mm and g0 = 25 mm

14 Eigenvalues of maglev system vs. lateral location of vehicle with h = 7 mm and g0 = 25 mm

15 Real part of eigenvalues of maglev system vs. lateral location of vehicle with h = 7 mm and g0 = 10, 15, 20, and 25 mm

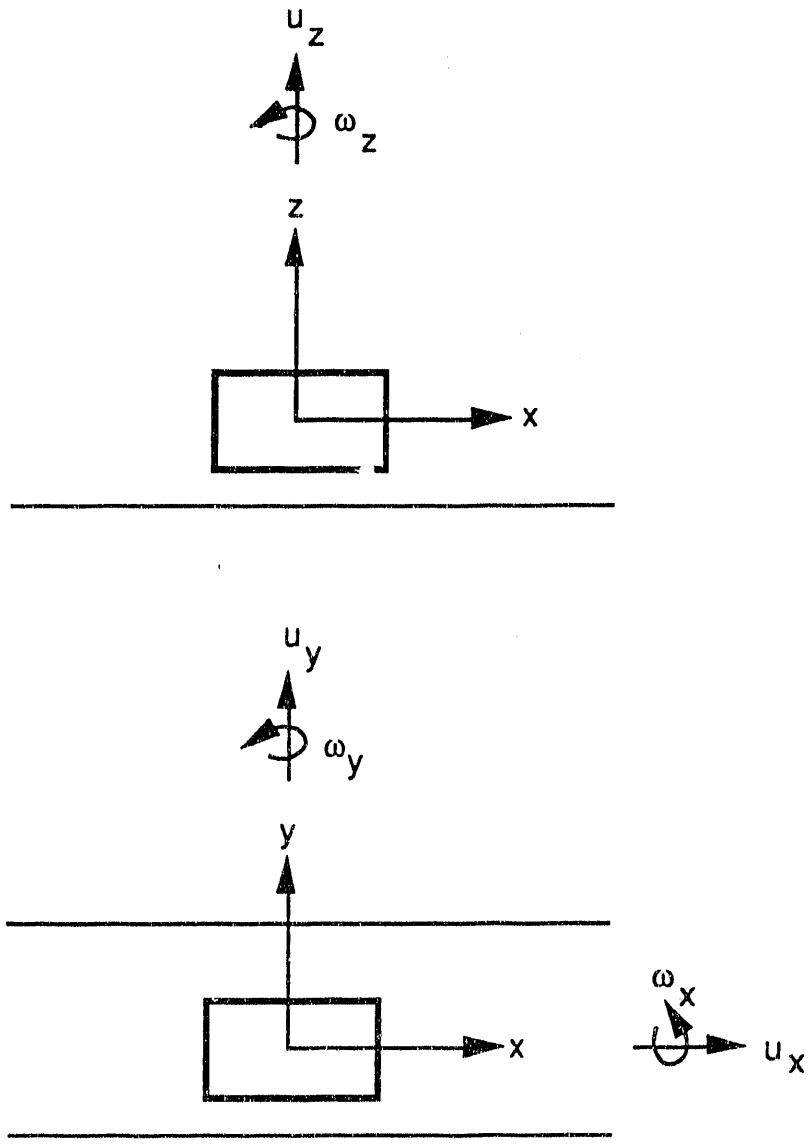

Fig. 1. Displacement Components of a Maglev System

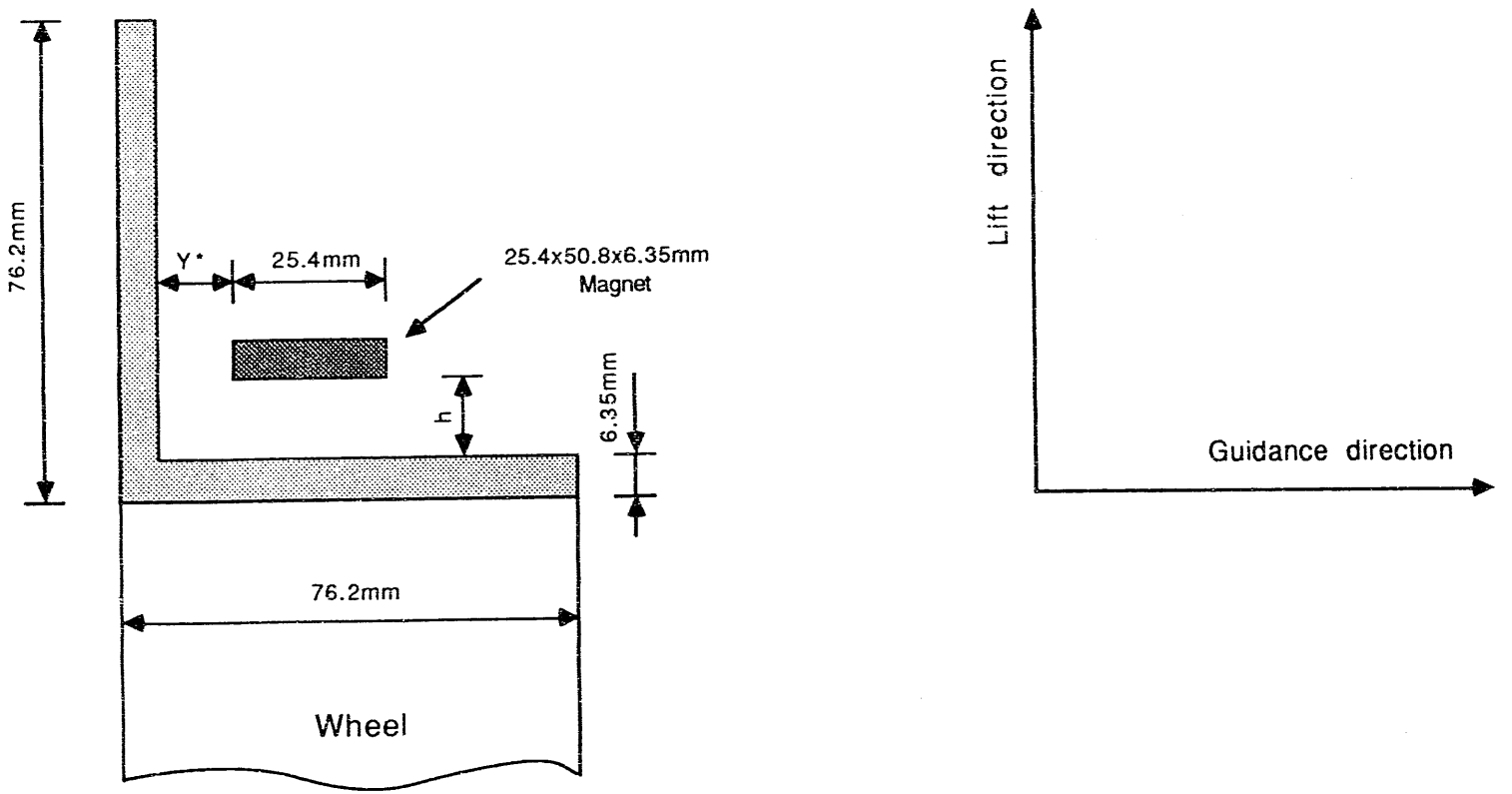

Figure 2 Schematic for magnetic force measurement on L-shape aluminum sheet guideway

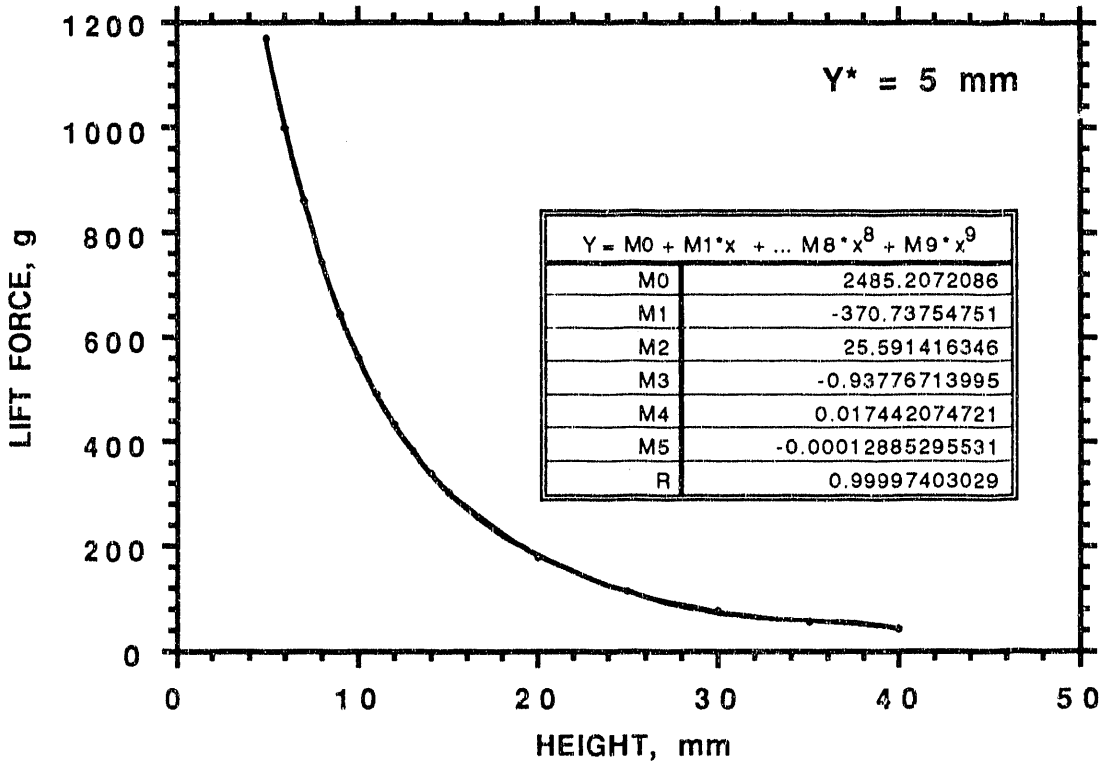
Y* = 5 mm
LIFT FORCE, g
HEIGHT, mm
1200
1000
800
600
400
200
0
0
10
20
30
40
50
Y = M0 + M1*x + ... M8*x^8 + M9*x^9
M0 2485.2072086
M1 -370.73754751
M2 25.591416346
M3 -0.93776713995
M4 0.017442074721
M5 -0.00012885295531
R 0.99997403029

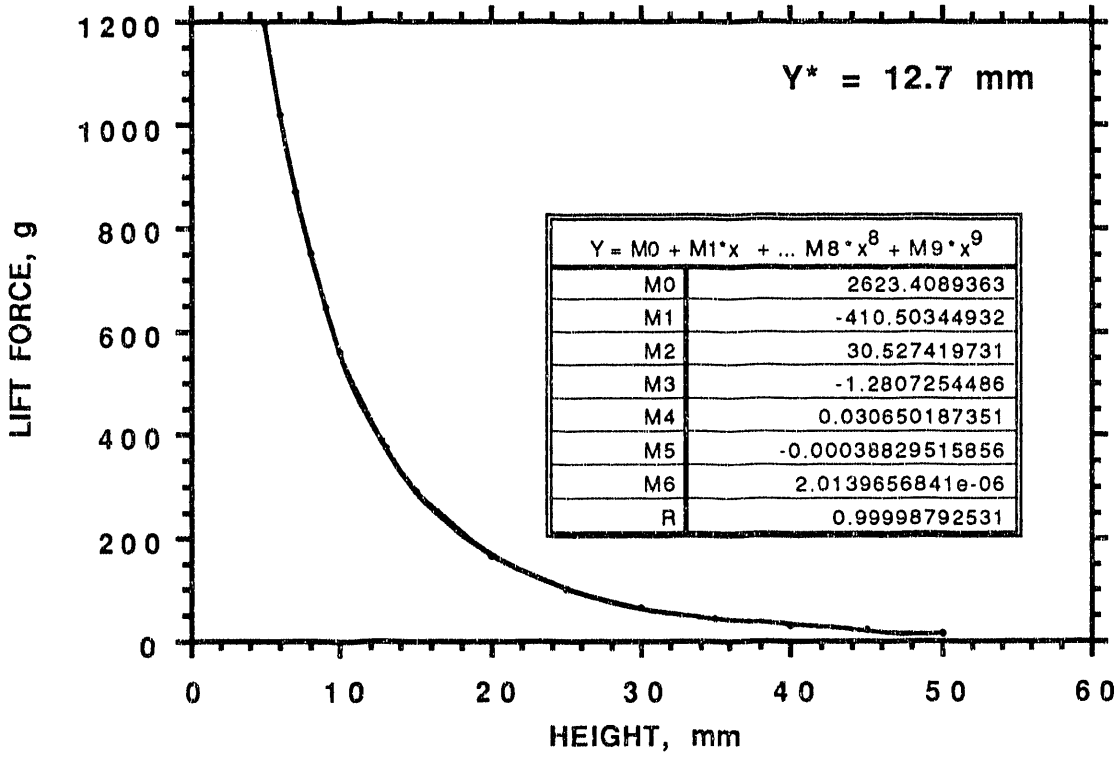

Y = M0 + M1*x + ... M8*x^8 + M9*x^9	
M0	2623.4089363
M1	-410.50344932
M2	30.527419731
M3	-1.2807254486
M4	0.030650187351
M5	-0.00038829515856
M6	2.0139656841e-06
R	0.99998792531

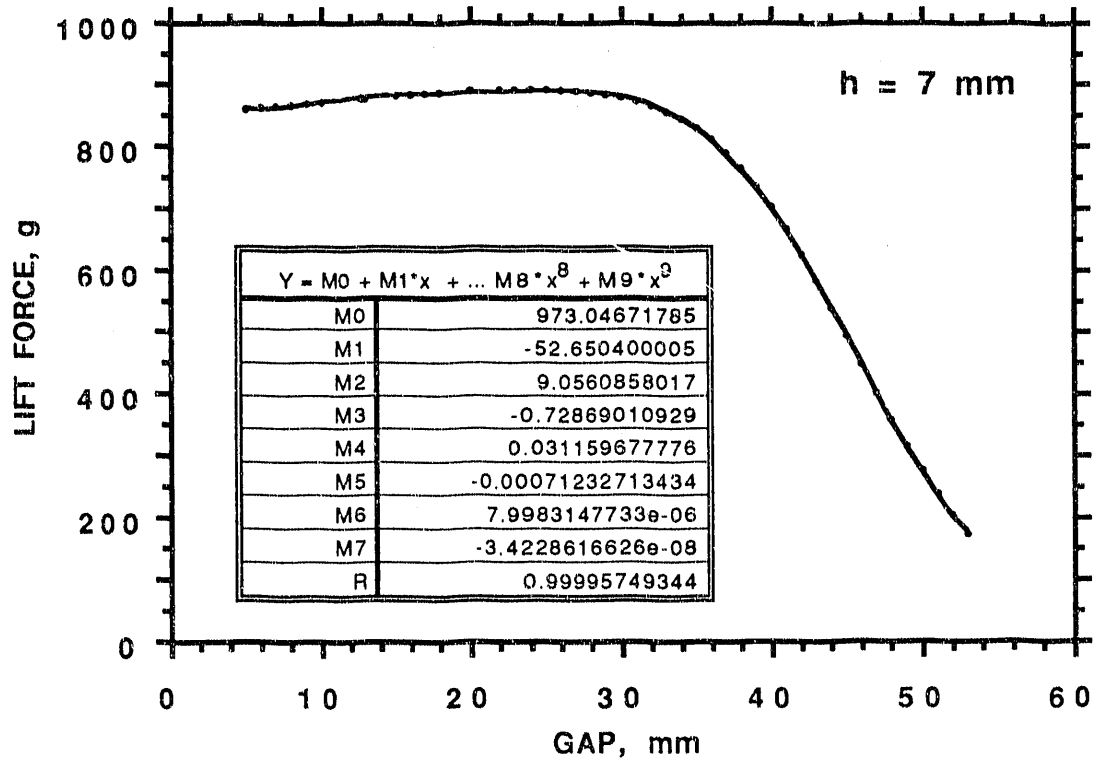

$Y = M0 + M1*x + \ldots M8*x^8 + M9*x^9$	
M0	973.04671785
M1	-52.650400005
M2	9.0560858017
M3	-0.72869010929
M4	0.031159677776
M5	-0.00071232713434
M6	7.9983147733e-06
M7	-3.4228616626e-08
R	0.99995749344

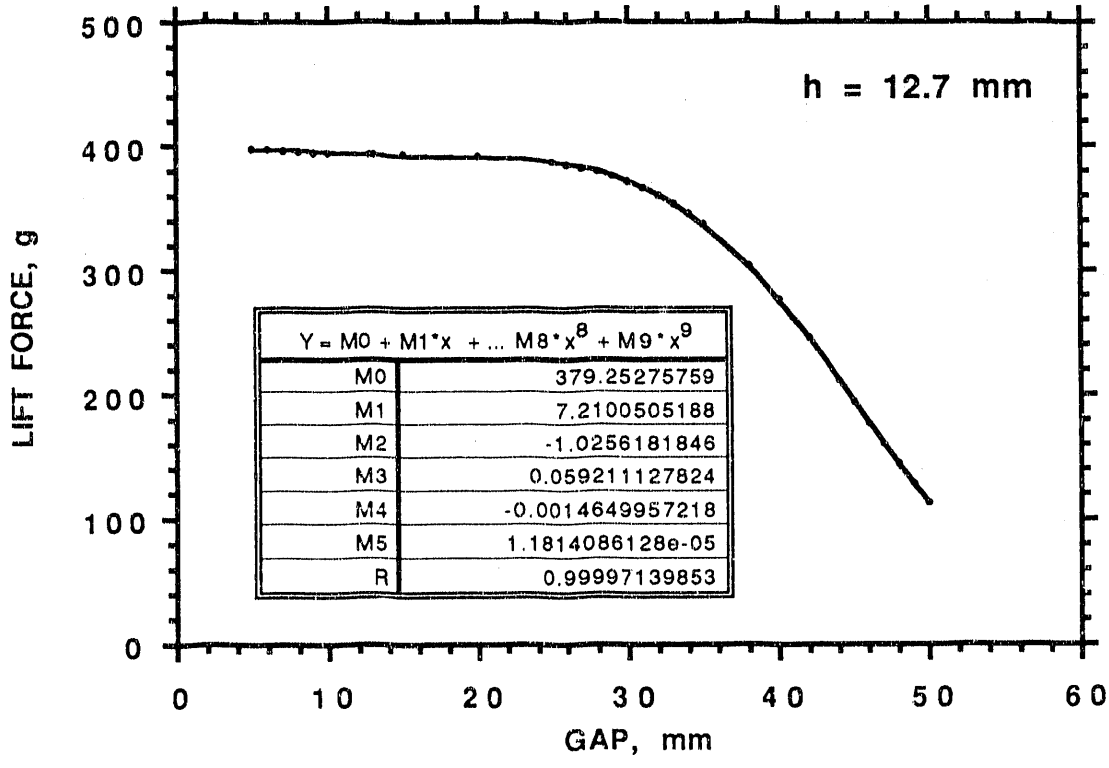

$Y = M0 + M1*x + \ldots M8*x^8 + M9*x^9$	
M0	379.25275759
M1	7.2100505188
M2	-1.0256181846
M3	0.059211127824
M4	-0.0014649957218
M5	1.1814086128e-05
R	0.99997139853

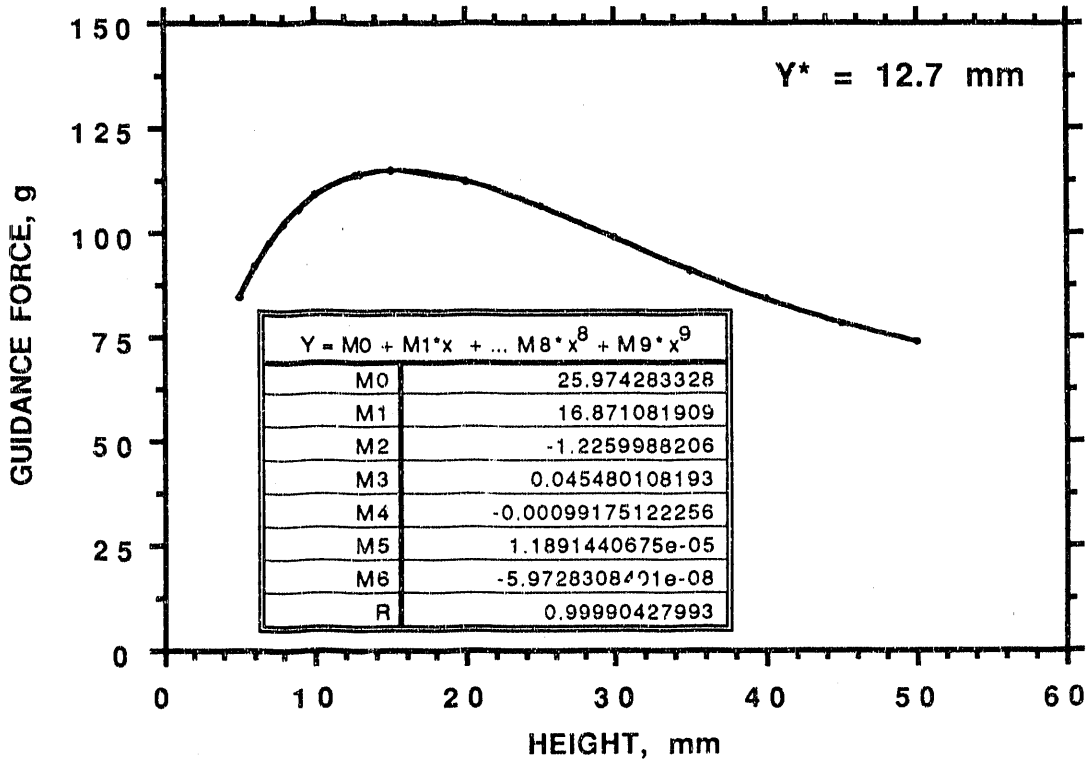

$Y = M0 + M1*x + \ldots M8*x^8 + M9*x^9$	
M0	25.974283328
M1	16.871081909
M2	-1.2259988206
M3	0.045480108193
M4	-0.00099175122256
M5	1.1891440675e-05
M6	-5.9728308401e-08
R	0.99990427993

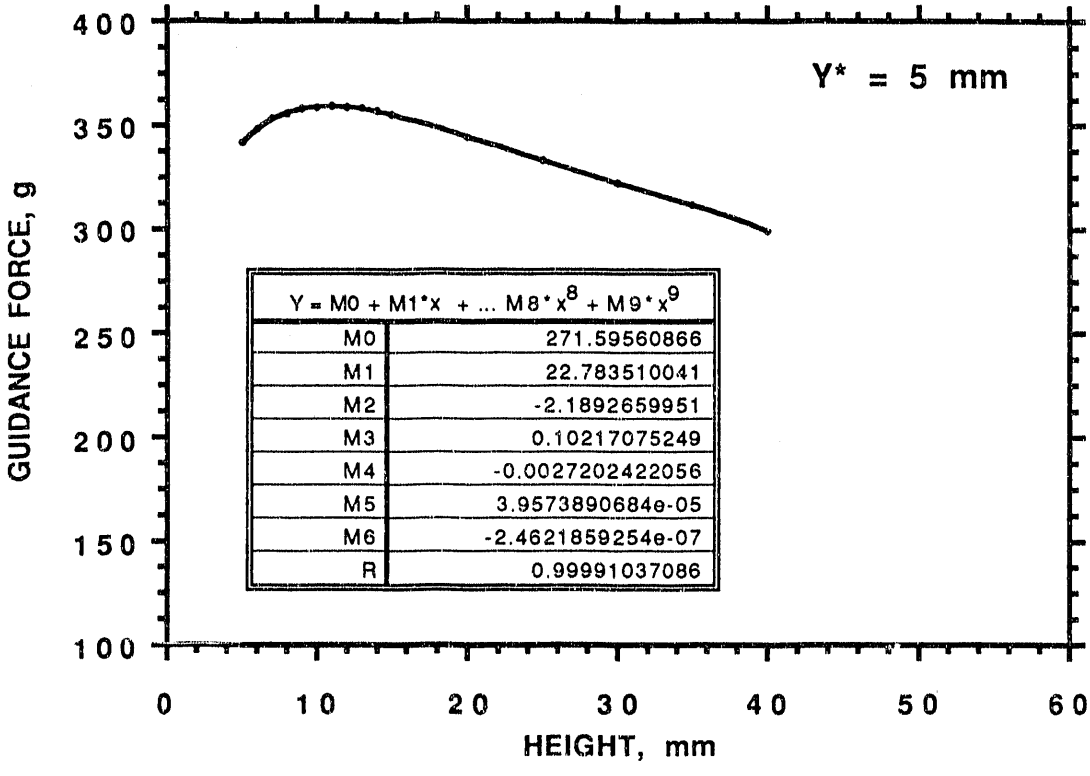

$Y = M0 + M1*x + \ldots M8*x^8 + M9*x^9$	
M0	271.59560866
M1	22.783510041
M2	-2.1892659951
M3	0.10217075249
M4	-0.0027202422056
M5	3.9573890684e-05
M6	-2.4621859254e-07
R	0.99991037086

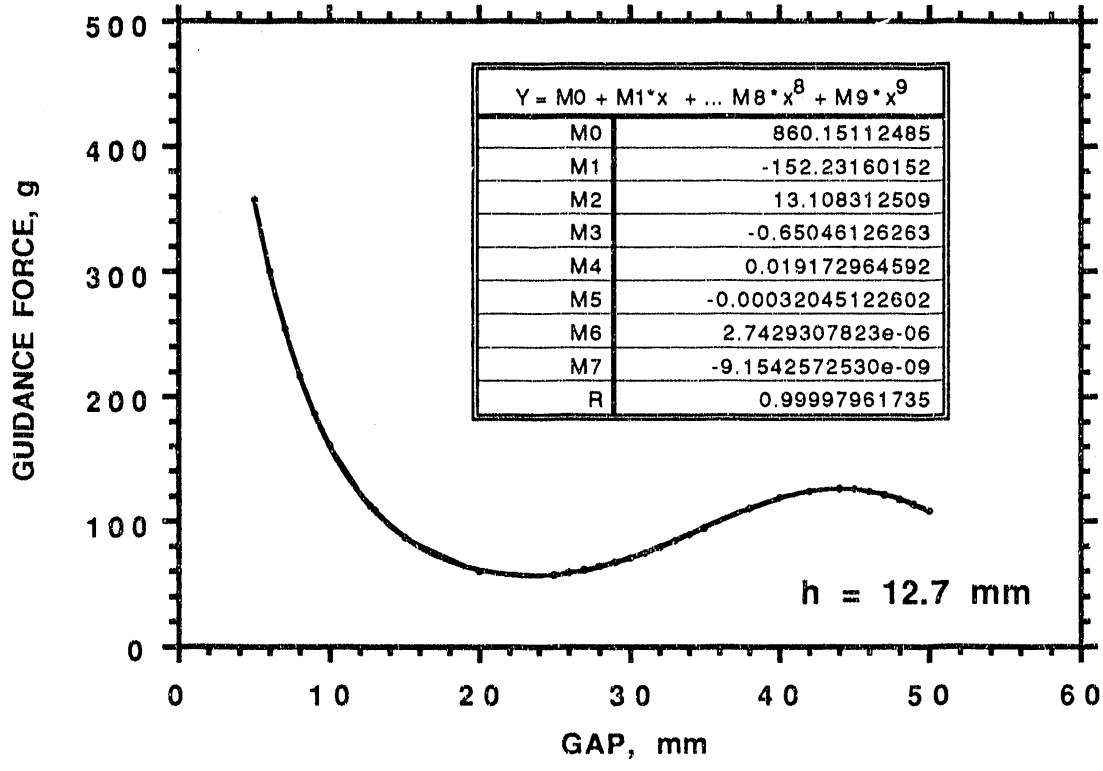

$Y = M0 + M1*x + \ldots M8*x^8 + M9*x^9$	
M0	860.15112485
M1	-152.23160152
M2	13.108312509
M3	-0.65046126263
M4	0.019172964592
M5	-0.00032045122602
M6	2.7429307823e-06
M7	-9.1542572530e-09
R	0.99997961735

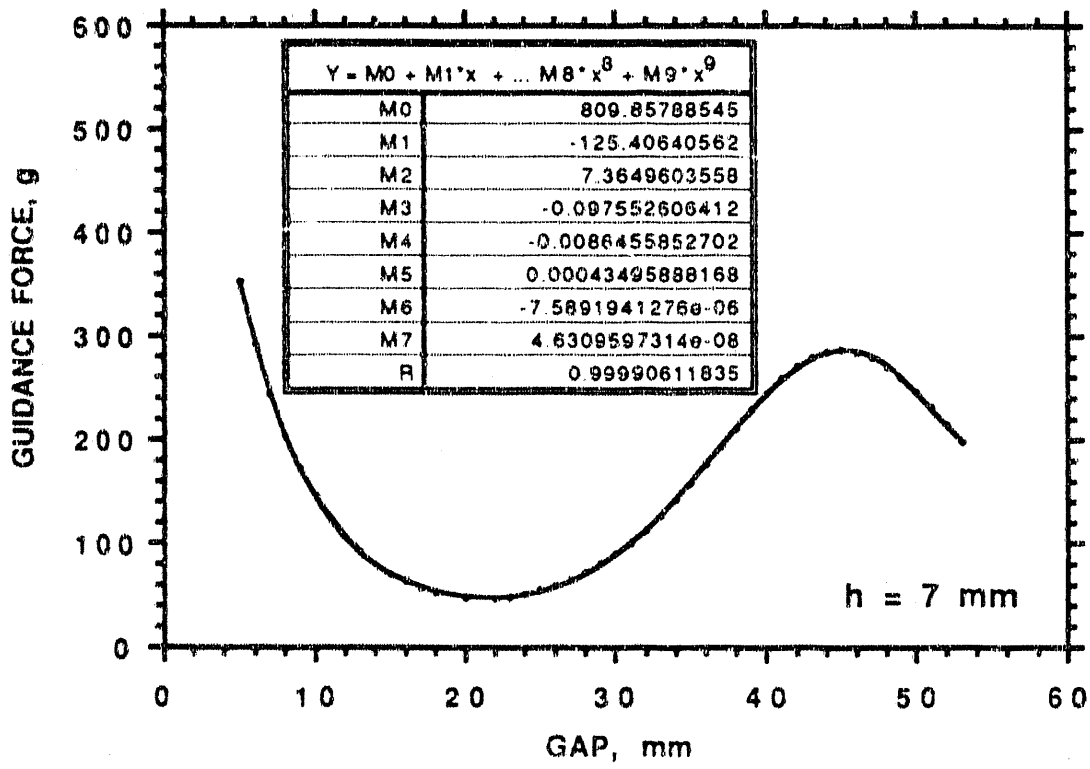
Y = M0 + M1*x + ... M8*x^8 + M9*x^9
M0 809.85788545
M1 -125.40640562
M2 7.3649603558
M3 -0.097552606412
M4 -0.0086455852702
M5 0.00043495888168
M6 -7.5891941276e-06
M7 4.6309597314e-08
R 0.99990611835
h = 7 mm
GUIDANCE FORCE, g
GAP, mm
0
100
200
300
400
500
600
0
10
20
30
40
50
60

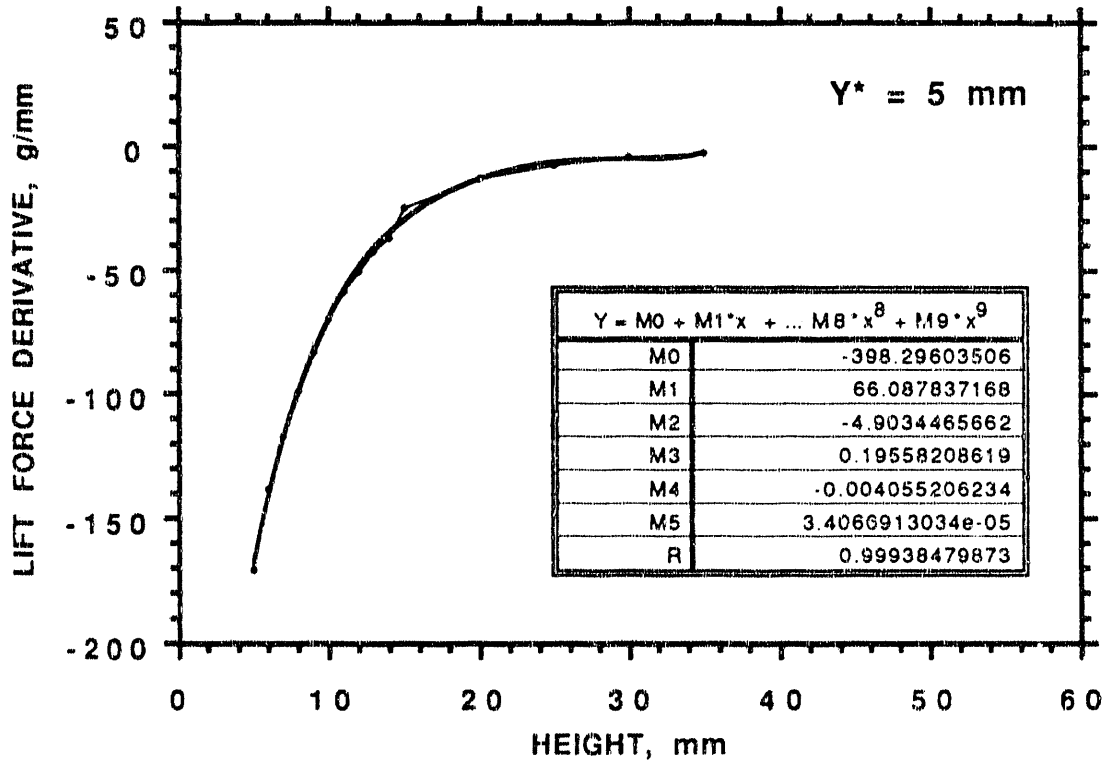
Y* = 5 mm
LIFT FORCE DERIVATIVE, g/mm
HEIGHT, mm
50
0
-50
-100
-150
-200
0
10
20
30
40
50
60
Y = M0 + M1*x + ... M8*x^8 + M9*x^9
M0 -398.29603506
M1 66.087837168
M2 -4.9034465662
M3 0.19558208619
M4 -0.004055206234
M5 3.4066913034e-05
R 0.99938479873

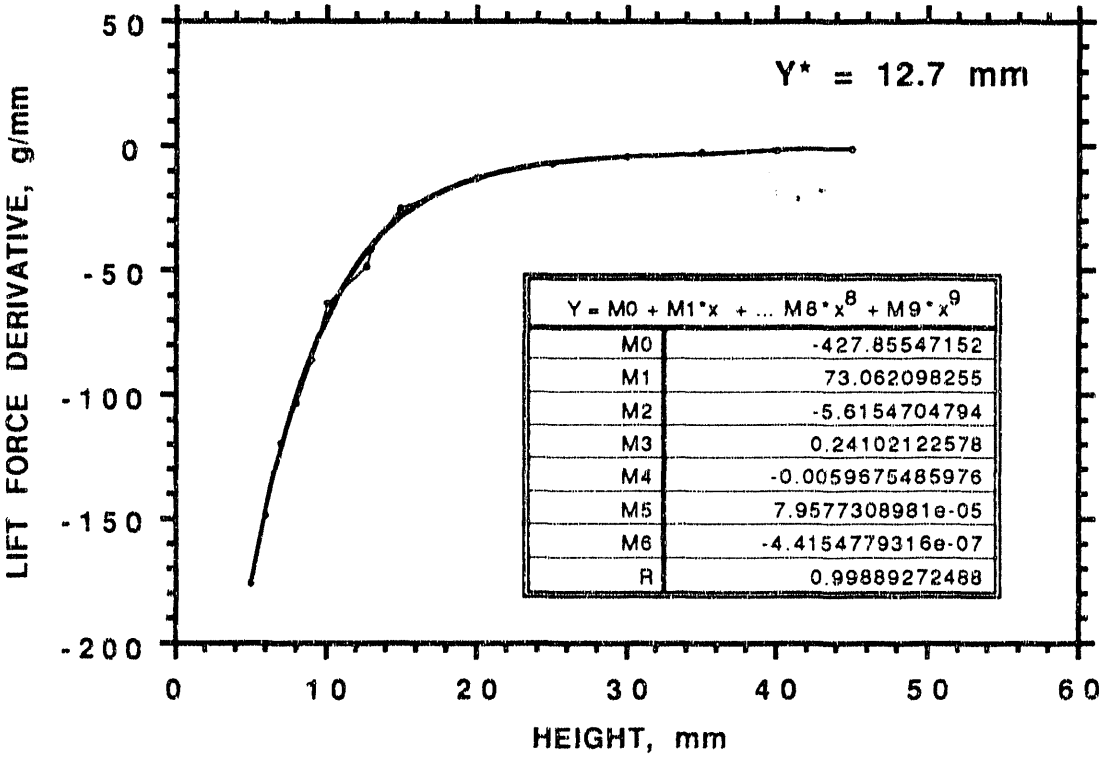

$Y = M0 + M1*x + \ldots M8*x^8 + M9*x^9$	
M0	-427.85547152
M1	73.062098255
M2	-5.6154704794
M3	0.24102122578
M4	-0.0059675485976
M5	7.9577308981e-05
M6	-4.4154779316e-07
R	0.99889272488

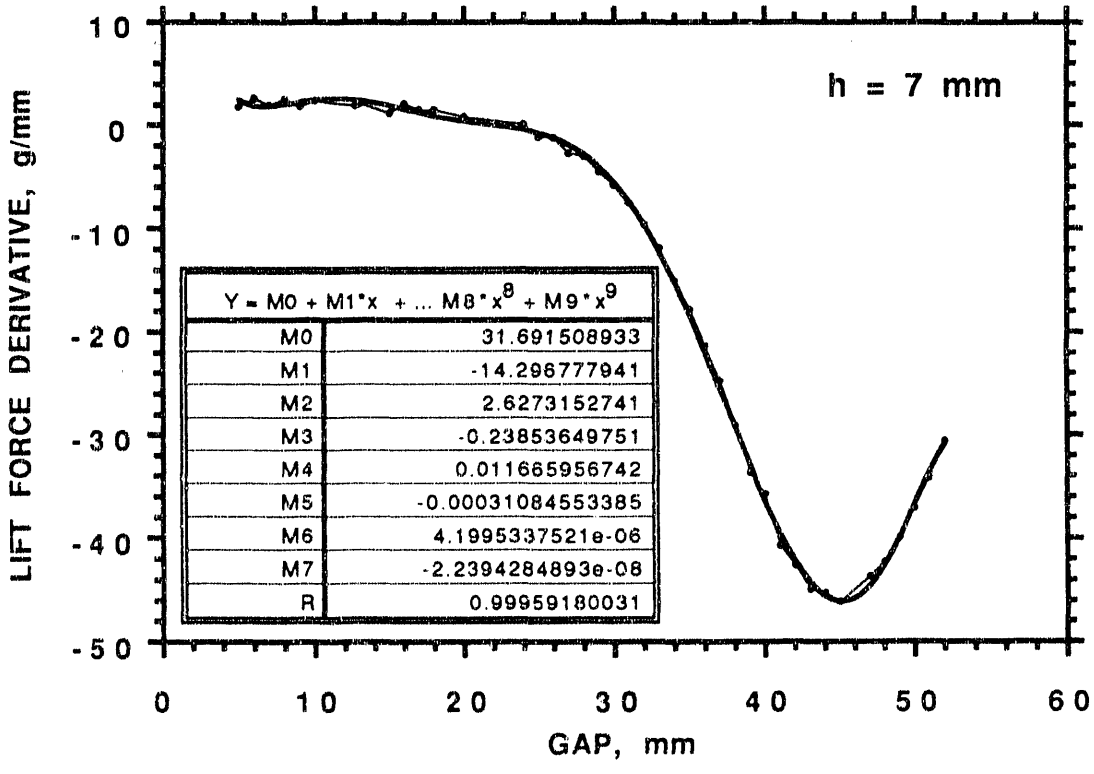
h = 7 mm
LIFT FORCE DERIVATIVE, g/mm
GAP, mm
10
0
-10
-20
-30
-40
-50
0
10
20
30
40
50
60
Y = M0 + M1*x + ... M8*x^8 + M9*x^9
M0 31.691508933
M1 -14.298777941
M2 2.6273152741
M3 -0.23853649751
M4 0.011665956742
M5 -0.00031084553385
M6 4.1995337521e-06
M7 -2.2394284893e-08
R 0.99959180031

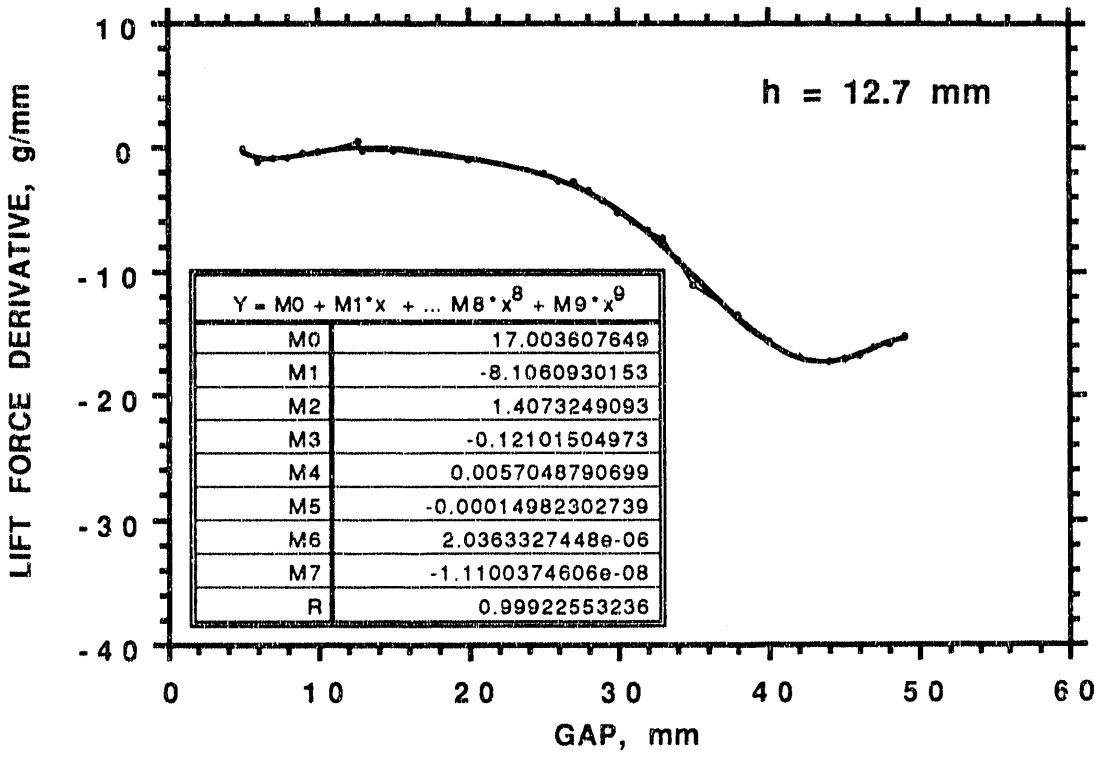

$Y = M0 + M1*x + \ldots M8*x^8 + M9*x^9$	
M0	17.003607649
M1	-8.1060930153
M2	1.4073249093
M3	-0.12101504973
M4	0.0057048790699
M5	-0.00014982302739
M6	2.0363327448e-06
M7	-1.1100374606e-08
R	0.99922553236

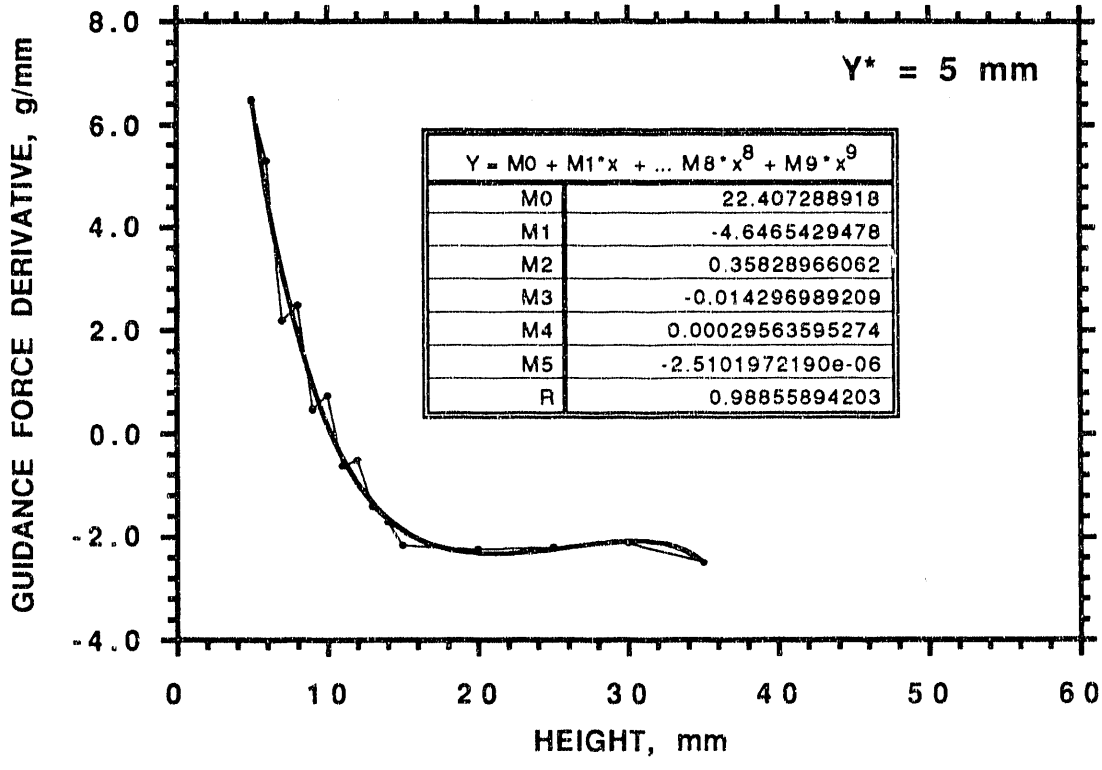

$Y = M0 + M1*x + \ldots M8*x^8 + M9*x^9$

M0	22.407288918
M1	-4.6465429478
M2	0.35828966062
M3	-0.014296989209
M4	0.00029563595274
M5	-2.5101972190e-06
R	0.98855894203

4 e

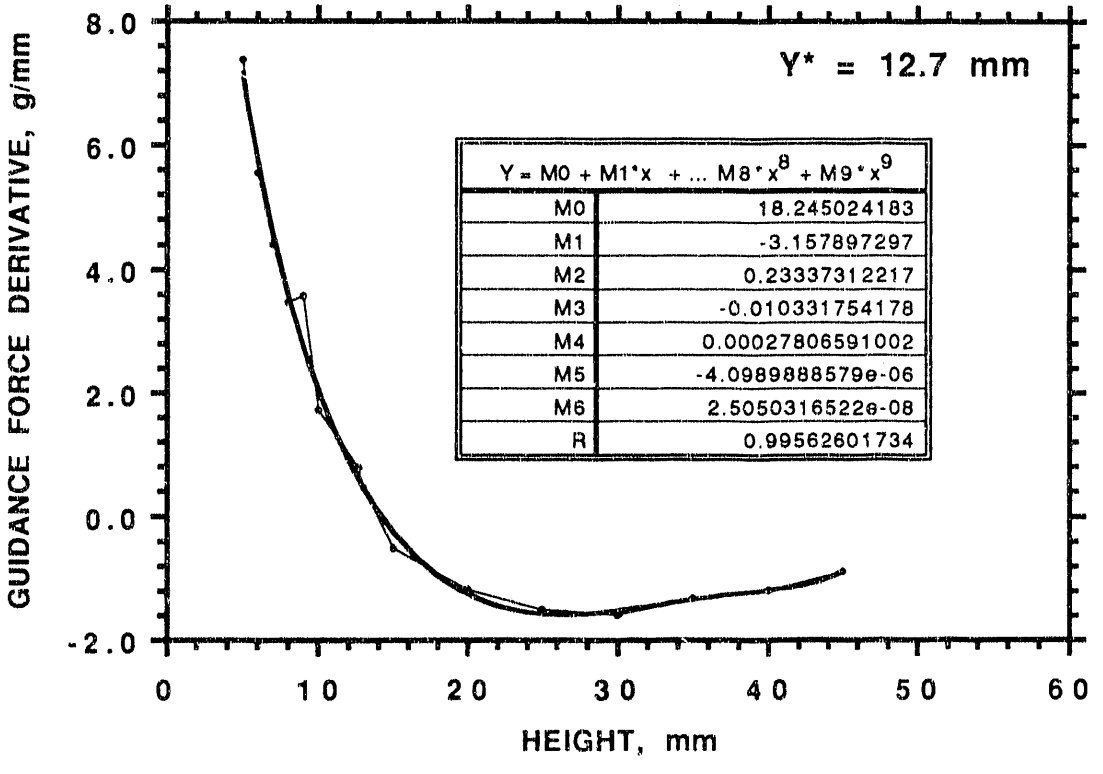

$Y = M0 + M1*x + \ldots M8*x^8 + M9*x^9$	
M0	18.245024183
M1	-3.157897297
M2	0.23337312217
M3	-0.010331754178
M4	0.00027806591002
M5	-4.0989888579e-06
M6	2.5050316522e-08
R	0.99562601734

4 f

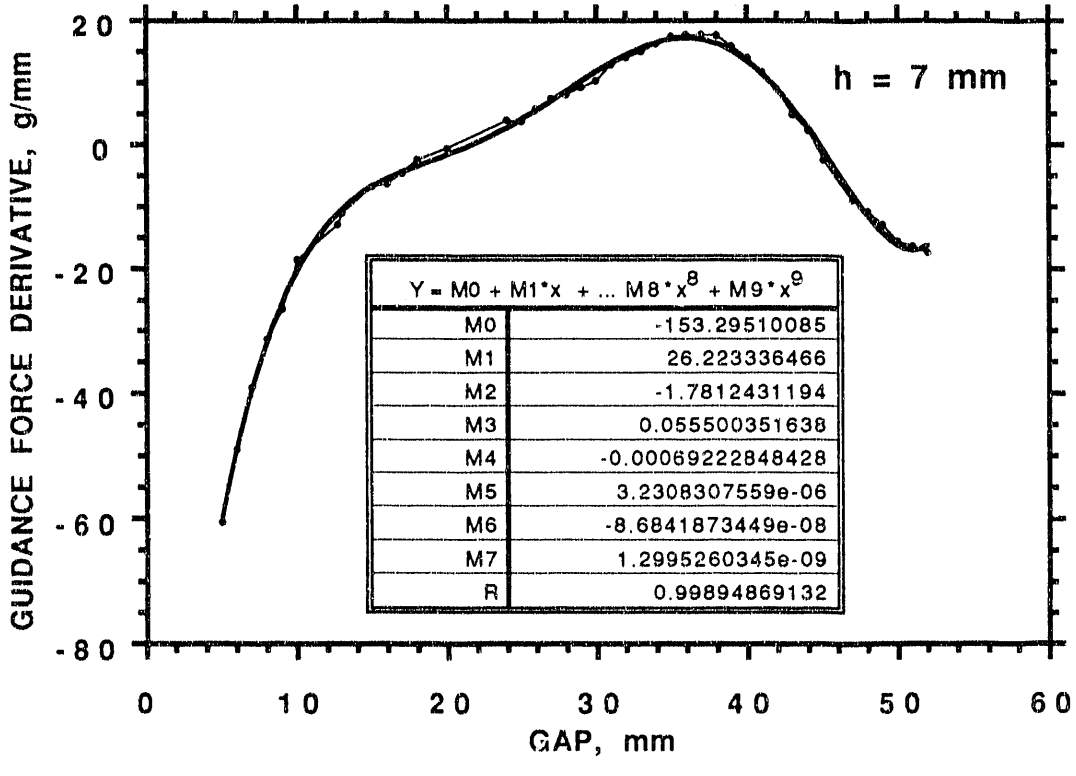

Y = M0 + M1*x + ... M8*x^8 + M9*x^9	
M0	-153.29510085
M1	26.223336466
M2	-1.7812431194
M3	0.055500351638
M4	-0.00069222848428
M5	3.2308307559e-06
M6	-8.6841873449e-08
M7	1.2995260345e-09
R	0.99894869132

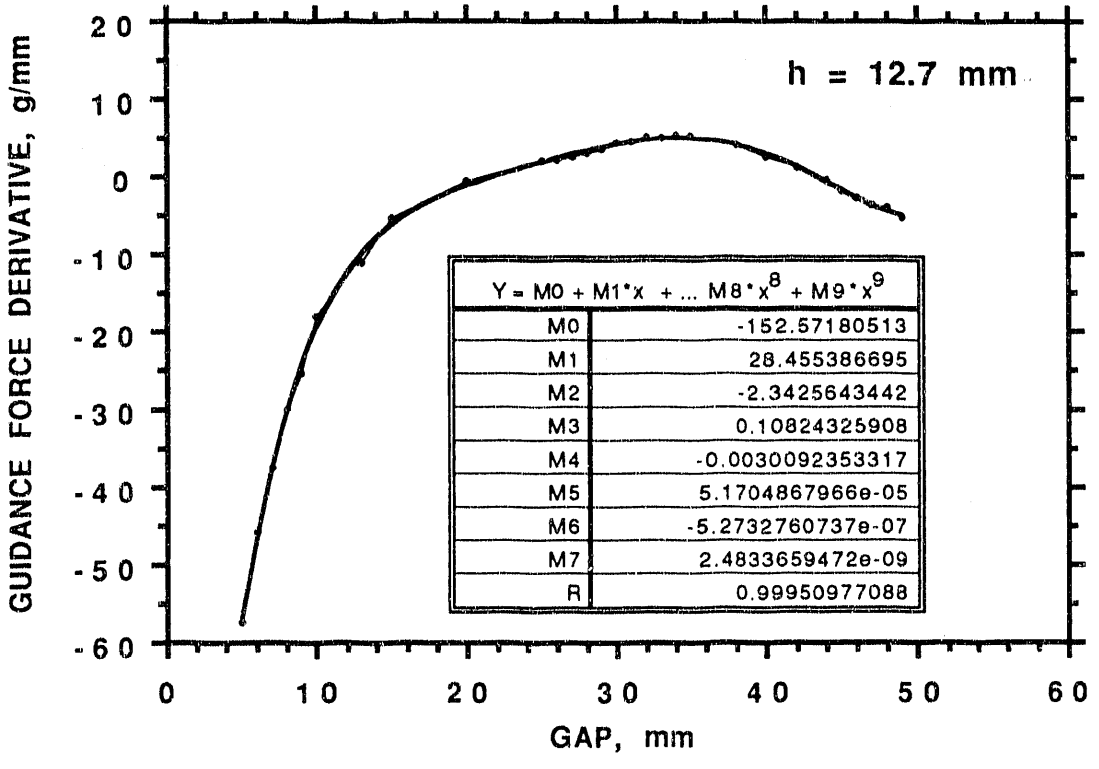

$Y = M0 + M1*x + \ldots M8*x^8 + M9*x^9$	
M0	-152.57180513
M1	28.455386695
M2	-2.3425643442
M3	0.10824325908
M4	-0.0030092353317
M5	5.1704867966e-05
M6	-5.2732760737e-07
M7	2.4833659472e-09
R	0.99950977088

4 h

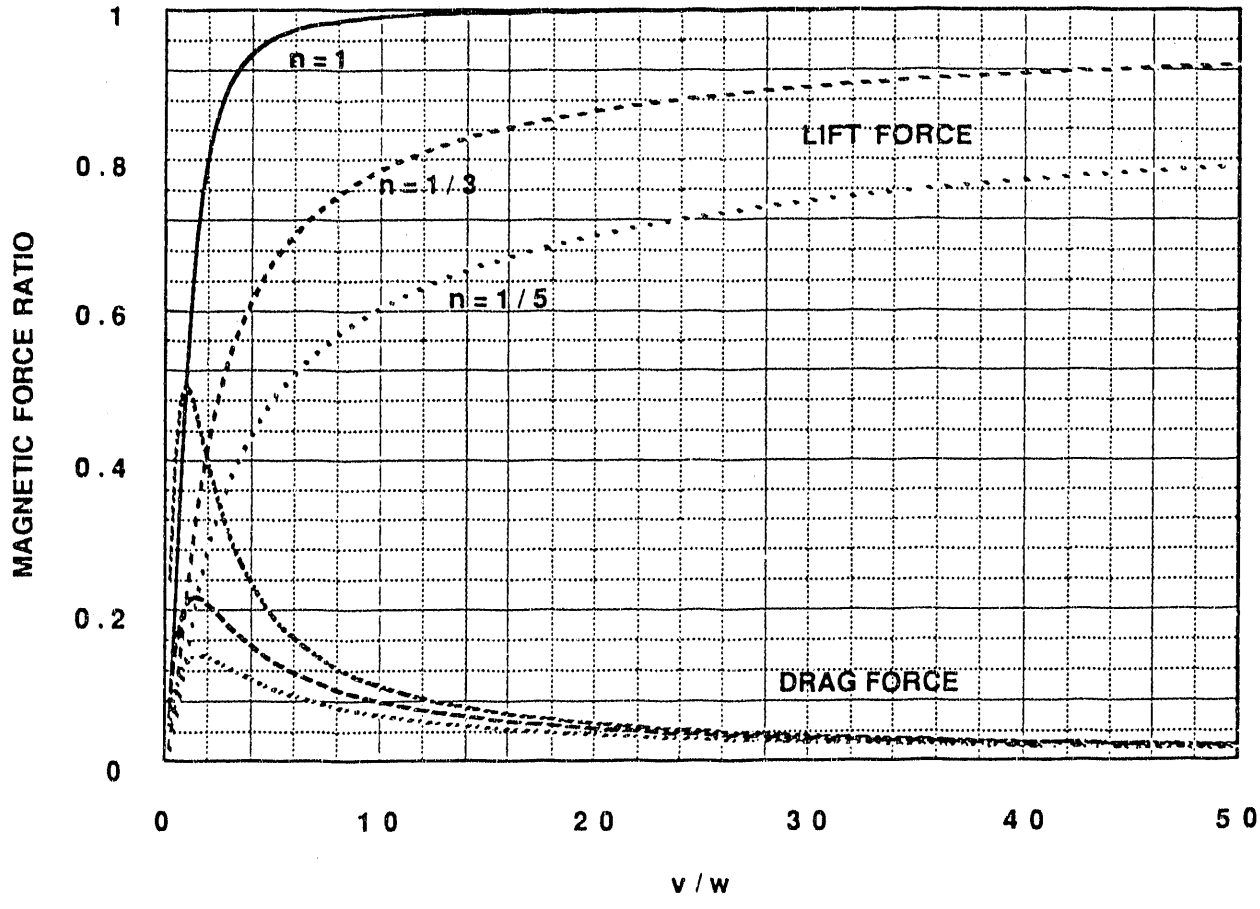

Fig. 2. Magnetic Forces Divided by Image Force

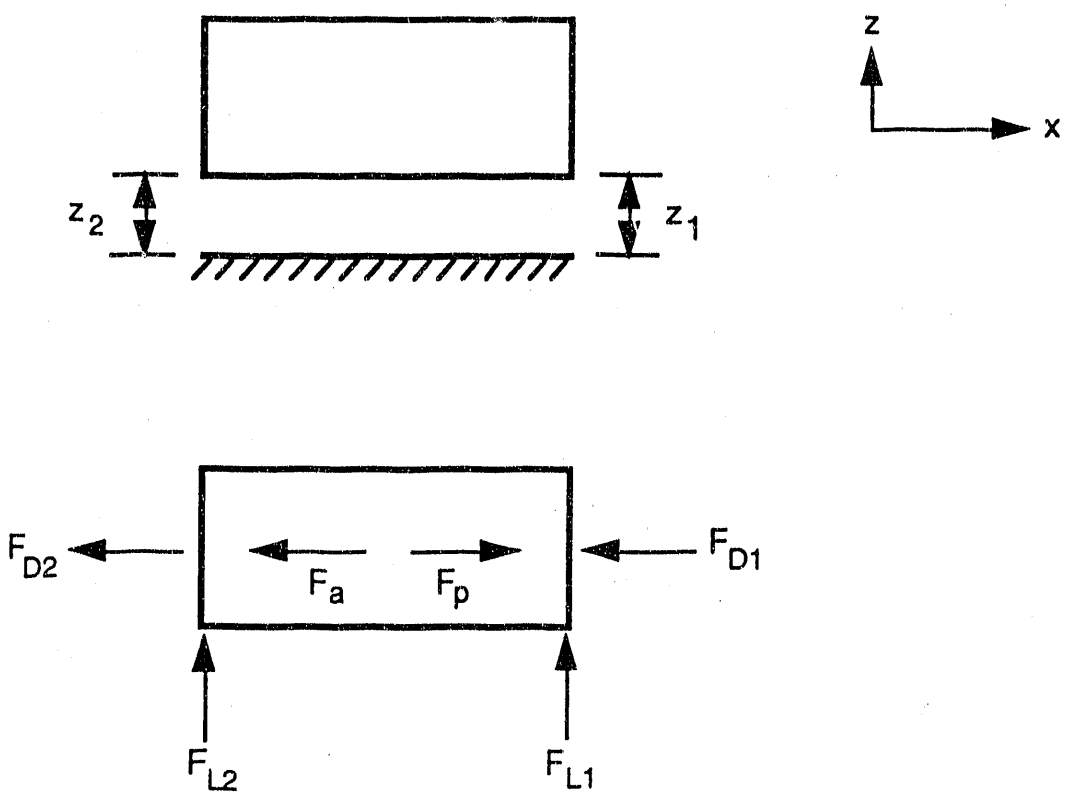

Fig. 4. A ~~Two~~ Three-Degree-of-Freedom Vehicle

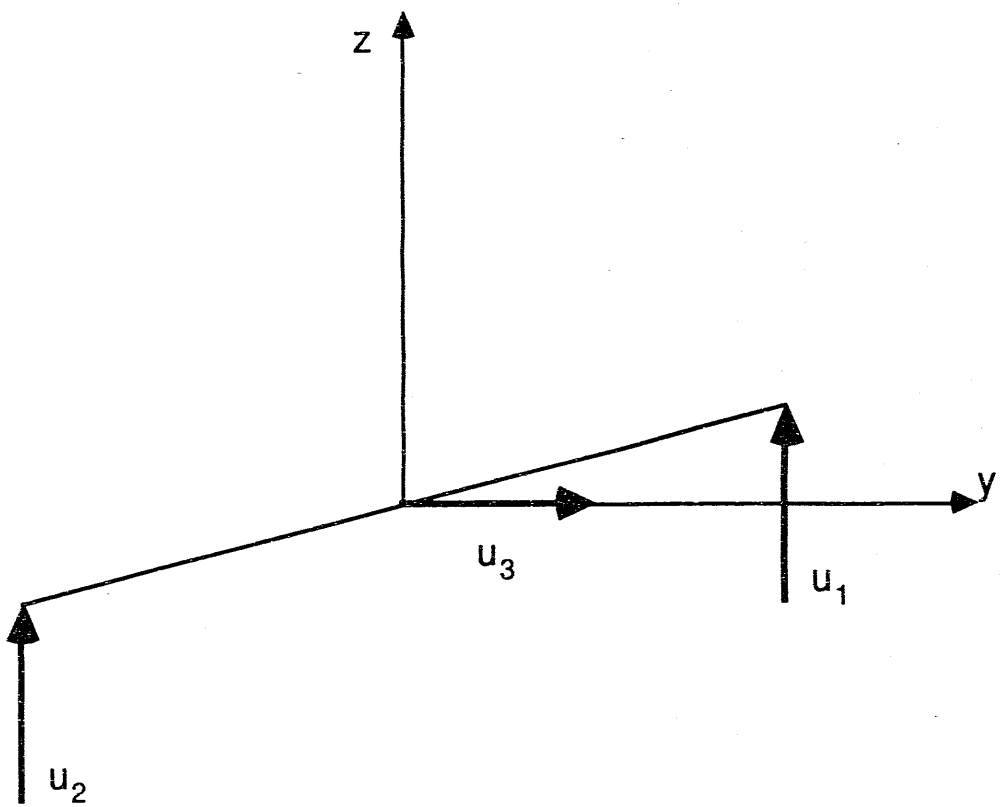

Figure 9 Displacement components of three-degree-of-freedom vehicle

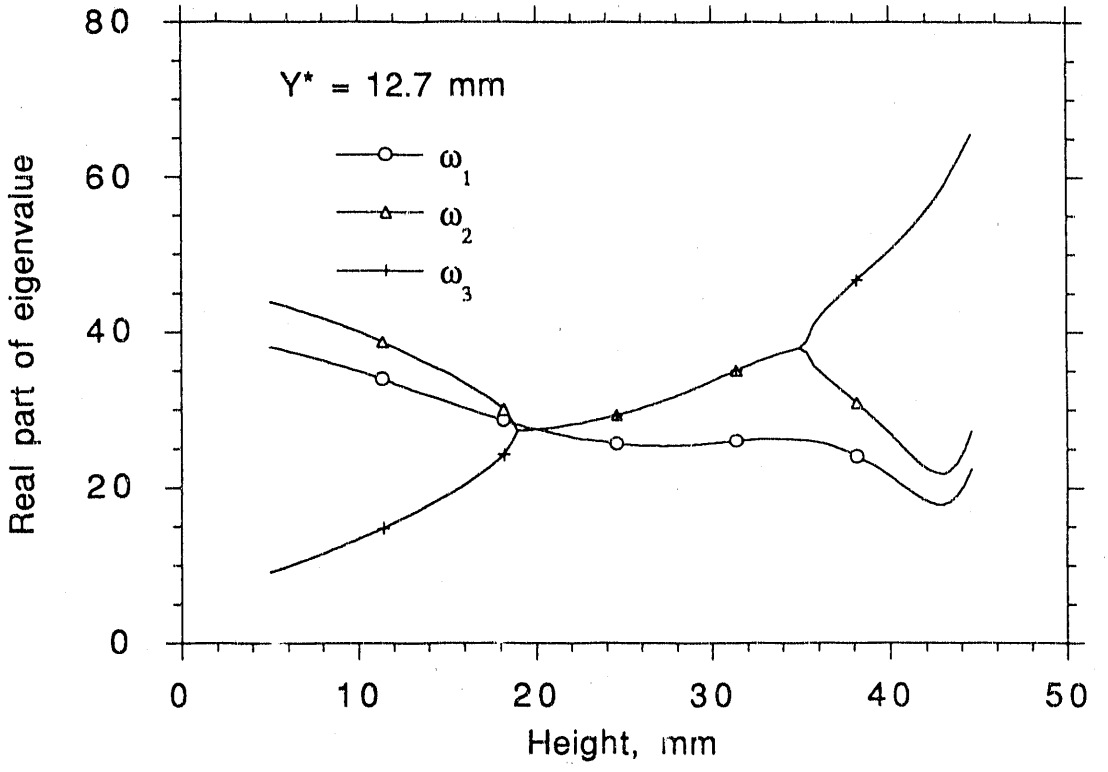
Y* = 12.7 mm
ω1
ω2
ω3
Real part of eigenvalue
80
60
40
20
0
0
10
20
30
40
50
Height, mm

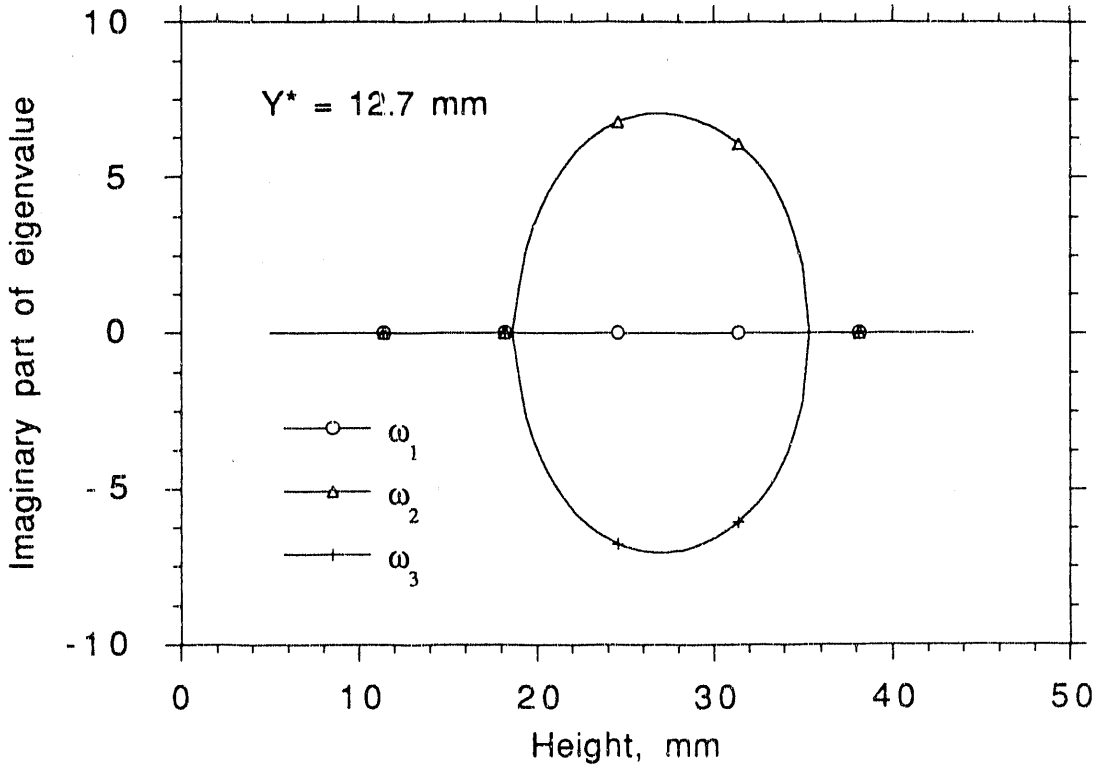
Y* = 12.7 mm
ω1
ω2
ω3
Imaginary part of eigenvalue
10
5
0
-5
-10
0
10
20
30
40
50
Height, mm

Fig 12

Uncoupled Heave Mode ω_1

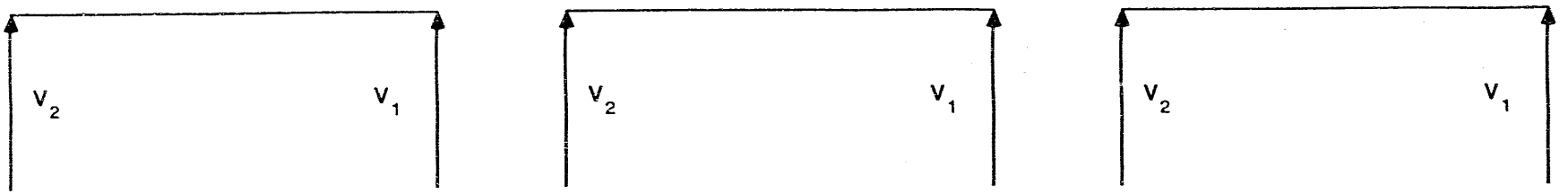

Coupled Roll-Yaw Mode ω_2

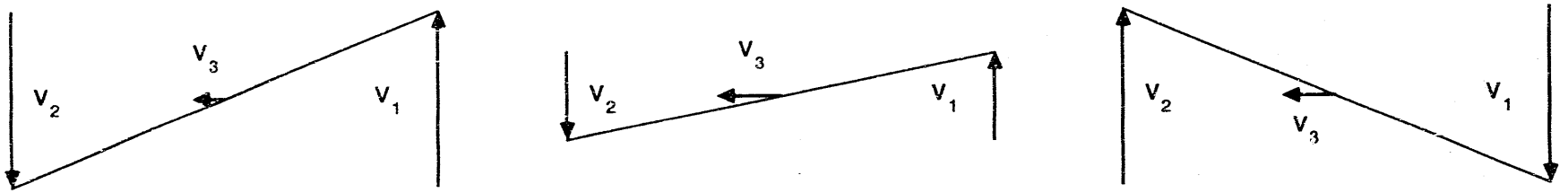

Coupled Roll-Yaw Mode ω_3

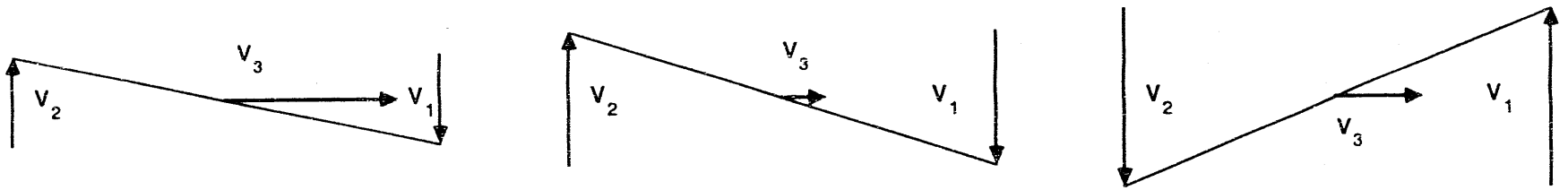

(a) h = 15 mm (b) h = 25 mm (c) h = 37 mm

Figure 11 Modal shapes of three-degree-of-freedom maglev system with Y* = 12.7 mm

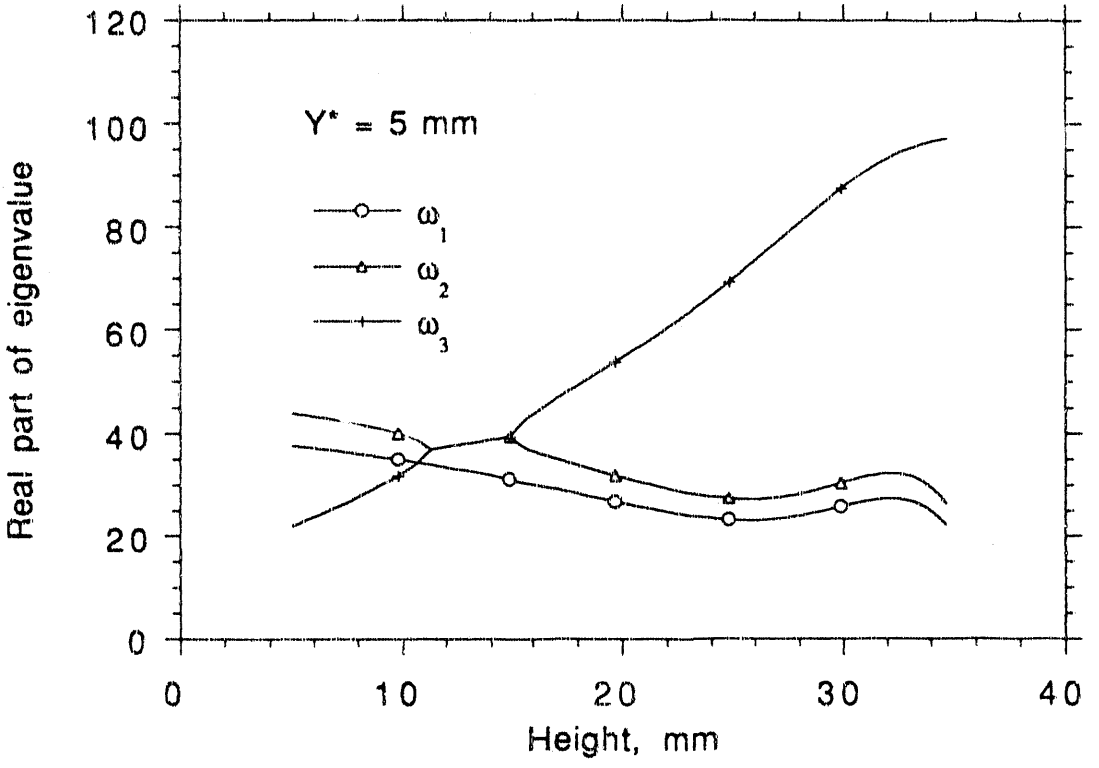
Y* = 5 mm
ω1
ω2
ω3
Real part of eigenvalue
120
100
80
60
40
20
0
0
10
20
30
40
Height, mm

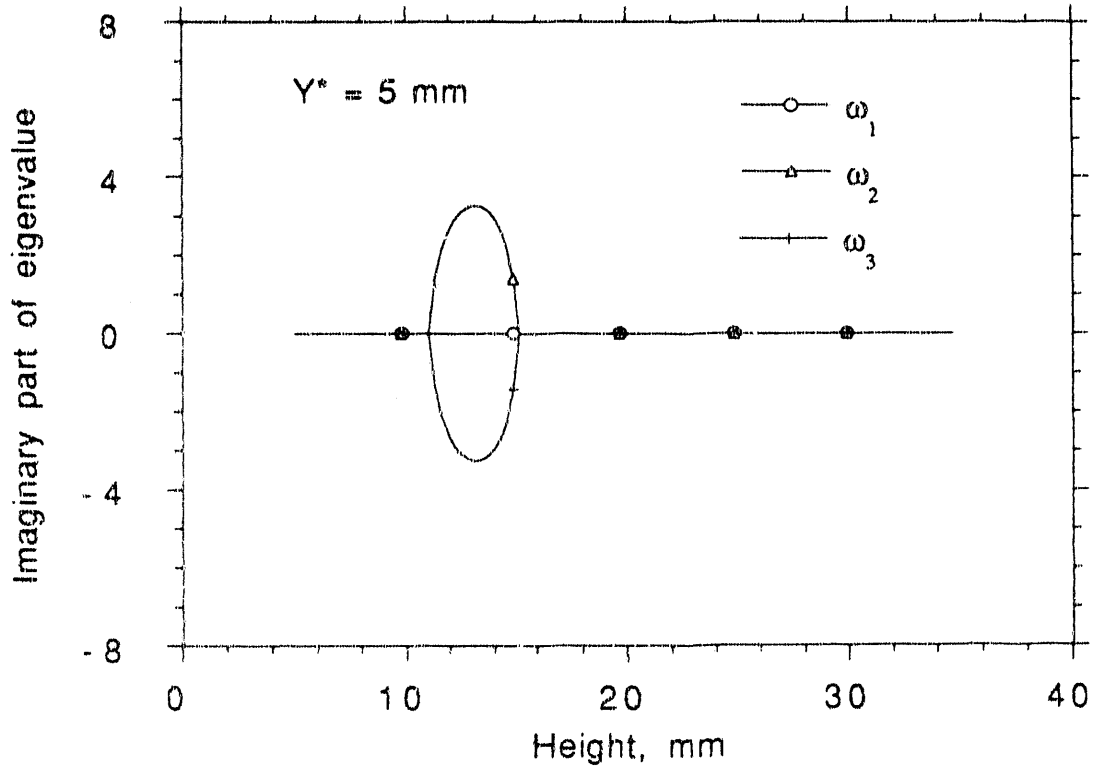
Y* = 5 mm
ω1
ω2
ω3
Imaginary part of eigenvalue
8
4
0
- 4
- 8
0
10
20
30
40
Height, mm

Fig 12

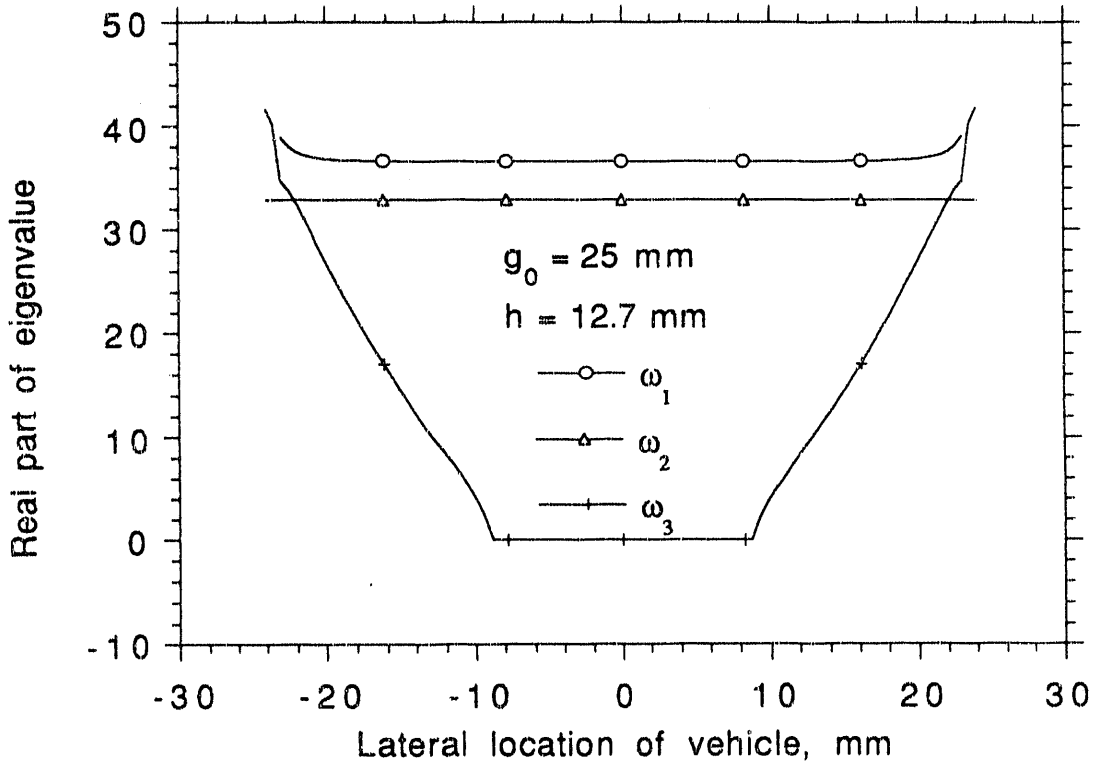
Real part of eigenvalue
50
40
30
20
10
0
-10
-30
-20
-10
0
10
20
30
Lateral location of vehicle, mm
g_0 = 25 mm
h = 12.7 mm
ω_1
ω_2
ω_3

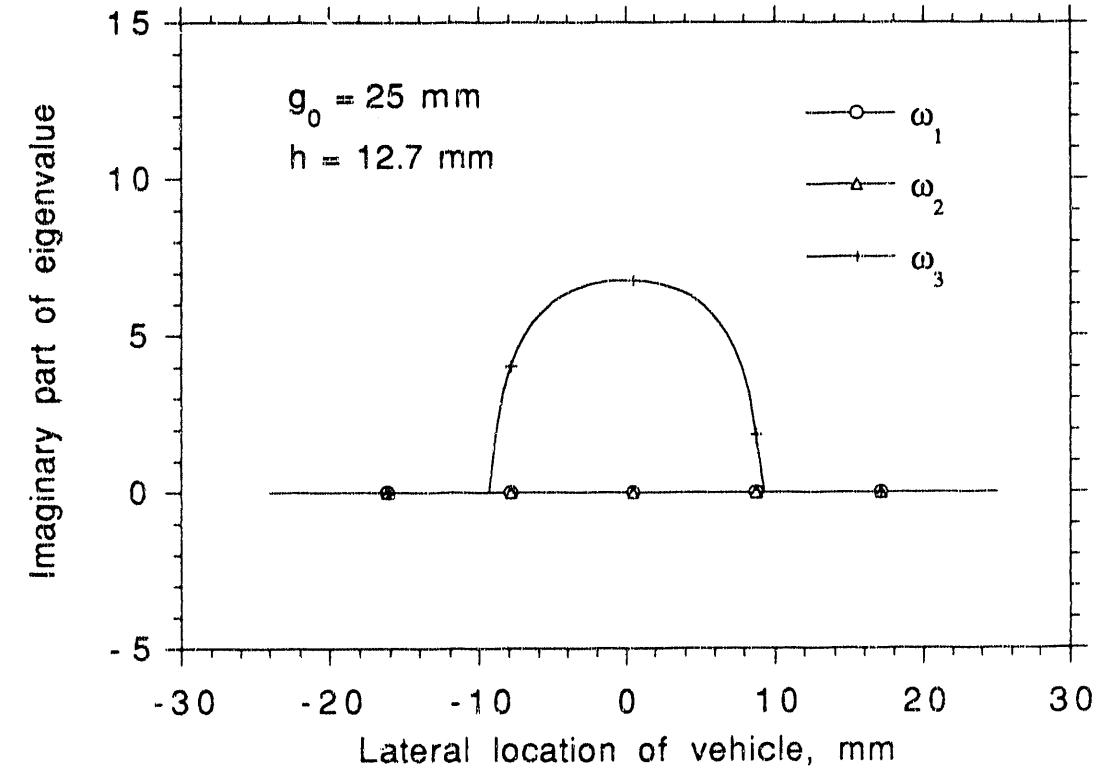
Imaginary part of eigenvalue
15
10
5
0
-5
-30
-20
-10
0
10
20
30
Lateral location of vehicle, mm
g_0 = 25 mm
h = 12.7 mm
ω_1
ω_2
ω_3

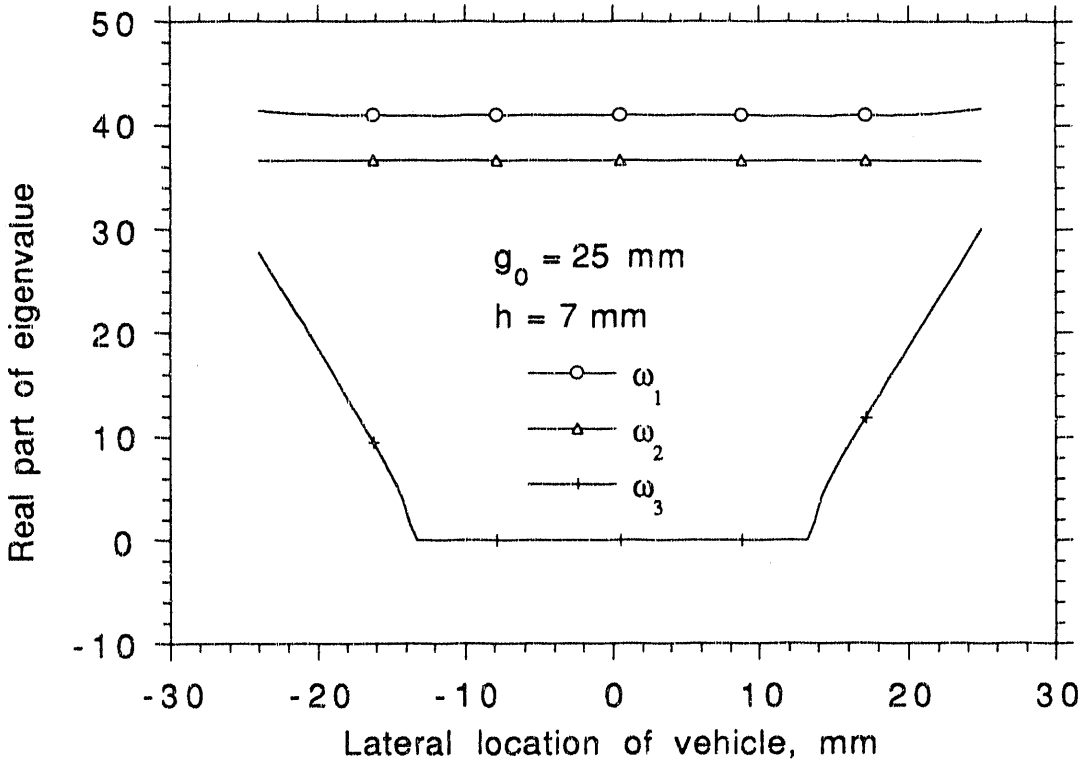
Real part of eigenvalue
50
40
30
20
10
0
-10
-30
-20
-10
0
10
20
30
Lateral location of vehicle, mm
g_0 = 25 mm
h = 7 mm
ω_1
ω_2
ω_3

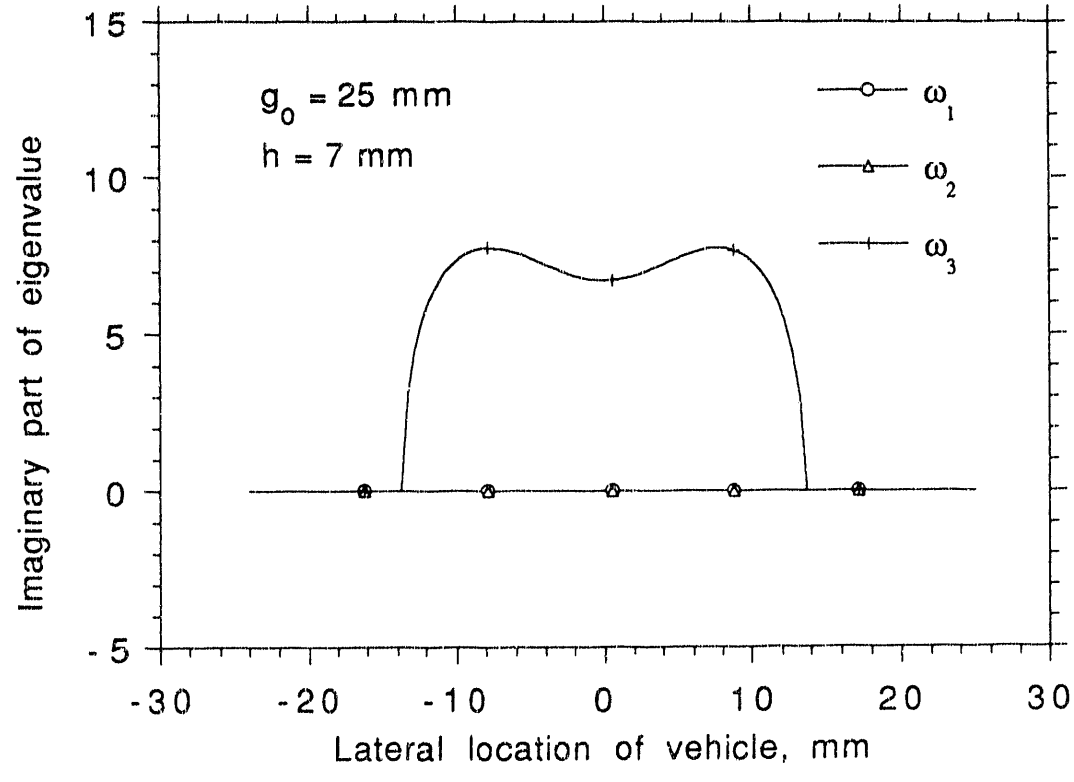
Imaginary part of eigenvalue
15
10
5
0
-5
-30
-20
-10
0
10
20
30
Lateral location of vehicle, mm
g_0 = 25 mm
h = 7 mm
ω_1
ω_2
ω_3

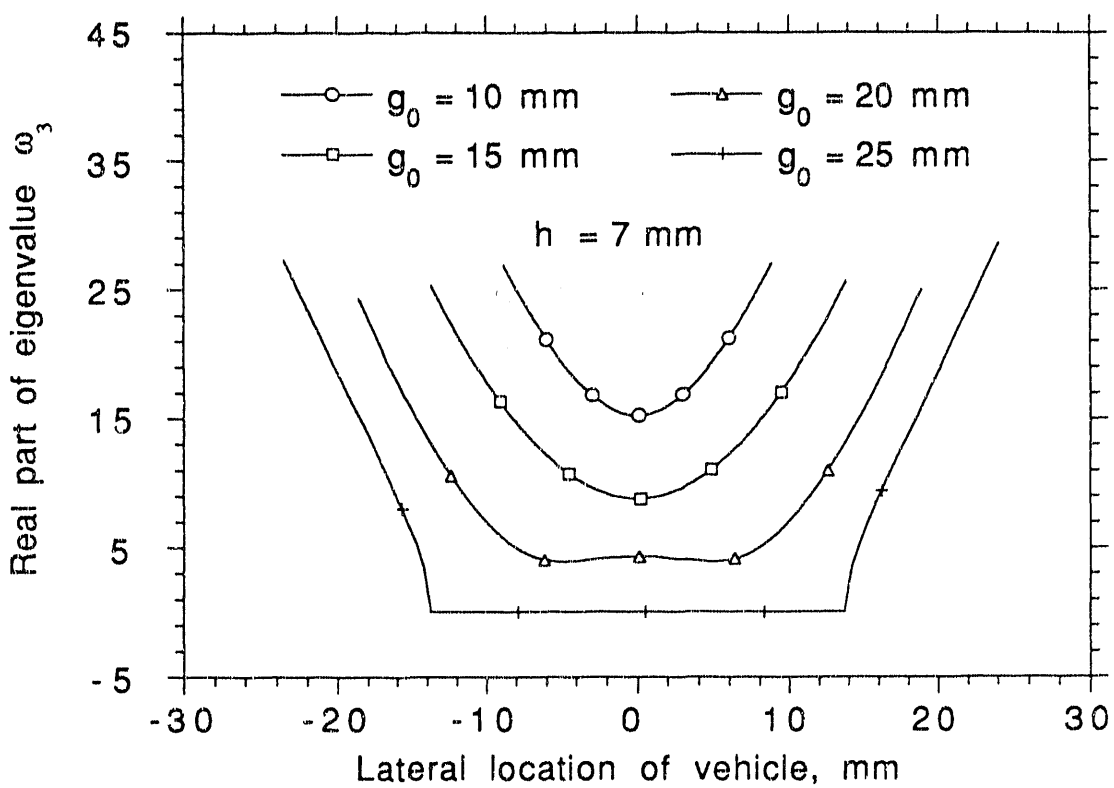
45
35
25
15
5
-5
-30
-20
-10
0
10
20
30
Real part of eigenvalue ω_3
g_0 = 10 mm
g_0 = 20 mm
g_0 = 15 mm
g_0 = 25 mm
h = 7 mm
Lateral location of vehicle, mm

Fig 15

END

DATE FILMED

12/8/92